Pro Gradu

Metal-nanoparticle-G4-DNA conjugates and their DC conductivity measurements

Teemu Parviainen

University of Jyväskylä
Department of Physics
Supervisors: Jussi Toppari & Alexander Kotlyar
March 2013

Preface

The work reviewed here has been carried out at Nanoscience Center at the Department of Physics in the University of Jyväskylä between May 2011 and December 2012 and in Tel Aviv University between June and July 2012.

I would like to thank my supervisor Dr. Jussi Toppari for giving me an excellent opportunity to work in Nanoelectronics research group with very interesting subjects. The working has been very rewarding for me and big part of this has been the company and guidance of Mr. Kosti Tapio and Mr. Shen Boxuan, in addition to all other co-workers in NSC. Also, I am very grateful to Dr. Alexander Kotlyar who provided me an unique chance to visit his research group in Tel Aviv University. This experience was unforgettable due to Your, Shay's and Gennady's gratuitous hospitality.

Financial support from the European Cooperation in Science and Technology (COST) for the travel and living expenses in Israel is gratefully acknowledged.

Studying in the University of Jyväskylä has been very enjoyable for me. The atmosphere here has been great due to many great friends who I have had a chance to meet here. I hope the friendships established here will be life-lasting.

Jyväskylä 22.3.2013

Teemu Parviainen

Abstract

Due to superior self-assembly properties, DNA is a very promising candidate for the basis of future bottom-up solutions for molecular electronics and therefore the conductivity of DNA is a very crucial question. In this work DC conductivity measurements on conjugates consisting of G-quadruplex DNA and metal nanoparticles were carried out. The fabrication and results obtained from the electrical measurements of three types of conjugates (20 nm G4-AgNP chains, 20 nm G4-AuNP flowers and 60 nm G4-AuNPs) are reported. Additionally, 20 nm AuNP chains coated with G4 were fabricated but not measured electrically. Results reported here indicate that in ambient conditions G4-DNA exhibits insulating behaviour with the resistance of the order of 1 TΩ. However, it was demonstrated that increasing the relative humidity affects to the intrinsic resistance of G4-DNA. The resistance of the conjugates was decreased down to 200 MΩ in the relative humidity of 80 %.

Tiivistelmä

Nykyisten mikropiirien valmistusmenetelmien kokoskaalojen rajat ovat lähestymässä, joten piirien tehojen kasvattamiseksi myös tulevaisuudessa vaihtoehtoisten menetelmien kehittämistä vaaditaan. Nanoteknologia tarjonnee ratkaisun tähän haasteeseen. Eräs erittäin mielenkiintoinen tulevaisuuden komponenttien perusta olisi DNA-molekyyli, jonka muokattavuus ja ylivoimaiset itsejärjestyvyysominaisuudet tarjoaisivat erittäin monipuolisen rakennuspalikan monenlaisiin käytännön sovelluksiin.

DNA-ketjujen sähköisten mittausten tulokset ovat kuitenkin vaihdelleet laidasta laitaan riippuen käytetyistä tutkimusasetelmista, mikä on hidastanut käytännön sovellusten kehittämistä. Epäsuorat mittaustavat, jotka keskittyvät DNA-liuosten spektroskopisten ominaisuuksien tutkimiseen, ovat antaneet tietoa mm. varauksen siirtymisprosessin tehokkuudesta, siihen liittyvistä aikaskaaloista sekä eri emässekvenssien vaikutuksesta varauksenkuljetukseen. Tulokset ovat nostaneet kysymyksiä varauksenkuljetukseen liittyvistä mekanismeista mutta yleisesti hyväksytyin ja helpoiten ymmärrettävä lienee malli, jossa DNA-ketjuun indusoitu elektroniaukko kulkeutuu lähinnä ns. ”G-hyppyjen” kautta, mikäli G-emästen välillä olevien A- ja T- emästen määrä on pieni. Jos G-emästen välillä on useita AT-emäksiä, voi myös A-emäs hapettua, jolloin varaus kulkeutuu termisten ”A-hyppyjen” kautta seuraavalle G-emäkselle. Todellisuudessa tilanne ei kuitenkaan ole aivan näin yksinkertainen, vaan DNA-juosteen emäksien muodostamaa π-pinoumaa täytyy tarkastella kokonaisuutena varauksen siirtymisen tehokkuuden kannalta.

Suurin osa tähän mennessä tehdyistä mittauksista on suoritettu tavallisilla kaksijuosteisilla DNA-ketjuilla, mutta aivan viime aikoina valmistusmenetelmien luotettavuuden paraneminen on mahdollistanut myös huomattavasti monimutkaisempien rakenteiden tuottamisen. Eräs erittäin mielenkiintoinen DNA-rakenne on G-johto, ts. G4-DNA, joka koostuu neljästä yhteen liittyneestä, pääasiassa G-emäksiä sisältävästä ssDNA-ketjusta. G-emäksen alhainen hapettumispotentiaali voisi mahdollistaa tällaisten rakenteiden erittäin hyvän sähkönjohtavuuden. Lisäksi G-johtojen on osoitettu olevan erittäin vakaita ra-

kenteita vaihtelevissa ympäristön olosuhteissa, joten niiden käyttö käytännön sovelluksissa voisi olla hyvinkin mahdollista.

Tässä opinnäytteessä esitellään tasajännite-sähkönjohtavuusmittauksia, joita tehtiin kolmelle erityyppiselle G4-DNA–metallinanopartikkeli-näytteelle. Näytteistä ensimmäinen koostui G4-DNA:lla yhteen liitetyistä 20 nm hopeananopartikkeleista (AgNP), toinen G4-päällystetyistä kukkamaisista 20 nm kultananopartikkelirakenteista (AuNP) ja kolmas G4-päällystetyistä 60 nm kultananopartikkeleista. Näytteet valmistettiin Alexander Kotlyarin laboratoriossa Tel Avivin yliopistossa osittain allekirjoittaneen toimesta. Lisäksi valmistettiin G4-päällystettyjä 20 nm AuNP-ketjuja mutta näille näytteille ei suoritettu sähköisiä mittauksia.

Konjugaatit loukutettiin kahden nanoelektrodin väliin dielektroforeesi-ilmiöön perustuen käyttäen vaihtuvaa sähkökenttää elektrodien välillä. Näin elektrodien välille kyettiin loukuttamaan jopa yksittäinen konjugaatti sähköisiä mittauksia varten, mikä todettiin atomivoimamikroskooppikuvantamisella.

G4-DNA–AgNP-ketjujen tapauksessa tulokset olivat selvästi muista poikkeavia. Normaaleissa huoneen olosuhteissa jännitealueella $-0{,}7$ - $0{,}7$ V ketjujen resistanssi oli luokkaa 1 kΩ, kun taas tämän jännitealueen ulkopuolella resistanssi kasvoi dramaattisesti luokkaan 1 TΩ. Siirtyminen pienestä sähköisestä vastuksesta suureen ja takaisin tapahtui reversiibelisti absoluuttisen jännitteen 0,7 V ympäristössä. Muilla näytteillä vastaavaa käyttäytymistä ei havaittu, vaan huoneen kosteudessa resistanssi oli aina luokkaa 1 TΩ. Pelkkien nanopartikkeleiden johtavuus vastaavissa olosuhteissa oli kuitenkin noin 1 kΩ, joten korkean johtavuuden tila G4-DNA–AgNP-ketjujen tapauksessa johtui luultavasti siitä, että metallipartikkelit pääsevät suoraan kontaktiin toistensa kanssa.

Ympäristön kosteuden vaikutusta 60 nm G4-DNA–AuNP-konjugaattien johtavuuteen tutkittiin tarkemmin nostamalla suhteellinen kosteusprosentti hiljalleen arvoon ~ 80 % ja mittaamalla jännite–virta-käyriä samanaikaisesti. Verrattuna paljaisiin elektrodeihin, joiden resistanssi väheni puhtaasti eksponentiaalisesti suhteellisen kosteuden kasvaessa, kosteuden vaikutus konjugaattien johtavuuteen oli huomattavasti suurempi suhteellisen kosteuden ollessa välillä 20 - 50 %. Paljaiden kultapartikkeleiden resistanssiin kosteudella ei ollut vaikutusta. Tulokset voidaan selittää ainakin G4-DNA-ketjujen sisäisen johtavuuden kasvamisella ympäristön kosteuden vaikutuksesta, sillä tunnetusti kosteudella on huomattava merkitys DNA-molekyylin konformaatioon. Tuloksen perusteella suhteellinen kosteus 50 % voisi olla G4-DNA-ketjulle ns. kriittinen kosteus, joka vaaditaan stabiloimaan sen rakenne.

Contents

1 Introduction

The self-assembly properties of DNA makes it a perfect candidate for the basis of future nanotechnological applications. It has already been demonstrated that DNA can act as a scaffold for complex structures .

A possibility to create nanoscale wires out of DNA would increase its usefulness tremendously. Electrical conductivity of DNA is a subject which has been under vigorous investigation during the past few decades. Results have shown insulating, semi-conducting and metallic behaviours depending on the composition of the DNA and measuring conditions. This indicates that the environmental conditions play a big role in the conformation of natural dsDNA and therefore in its charge carrying capacity. Measurements have been done both in liquid and dry conditions on different substrates. In ambient conditions stabilizing ions are not available and the two strands forming the dsDNA tend to repel each other making the conditions for charge transfer through the molecule more unfavourable. Also properties of the substrate can affect the DNA conformation. This could be the main reason why natural dsDNA in an ambient environment and on substrates (e.g. SiO_2 and mica) is a poor conductor.

In order to solve the issue of conformational changes it is proposed to use that more stable DNA-structures, such as M-DNA and G4-DNA. Especially G4-strands have been shown to be very stable in different conditions. Additionally, the high content of G-nucleotides, known to have the lowest ionization potential among the nucleotides, makes these structures very promising candidates for future bottom-up nanoelectronic applications.

In this thesis synthesis and electrical DC conductance measurements in ambient conditions of various G4-DNA-metal conjugates are studied and discussed. The conductance was measured from conjugates immobilized between two fingertip-like gold-nanoelectrodes by dielectrophoresis. As stated, these kind of measurements have a high relevance in respect to the industrial applications of DNA molecules.

2 Background

2.1 DNA structure

2.1.1 Nucleotides

Nucleotides have very essential roles in cellular metabolism. They are used for example in the storage of chemical energy in the form of ATP-molecule, response of cells to various extracellular stimuli and structural elements of an array of enzyme cofactors and metabolic intermediates. However, the most interesting function of nucleotides in respect to this thesis is being a constituent of nucleic acids. Deoxyribonucleic acid (DNA) and ribonucleic acid (RNA) are the carriers of genetic information, therefore containing the essential information for the production of every protein and ultimately of every biomolecule and cellular component. It is not easy to emphasize enough the huge role of the nucleic acids as the building blocks of the life.

Nucleotides are composed of three components which are presented in Figure 2.1. In the case of DNA-nucleotide the basis consists of a cyclic 2'-deoxy-D-ribose-sugar and a phosphate group, PO_4^{2-}. In RNA the sugar group is correspondingly D-ribose. Nucleotides form polymers when the OH-group connected to the 3' carbon atom of the pentose reacts with the phosphate-group of other nucleotide forming a covalent phosphodiester-bond. Therefore, the

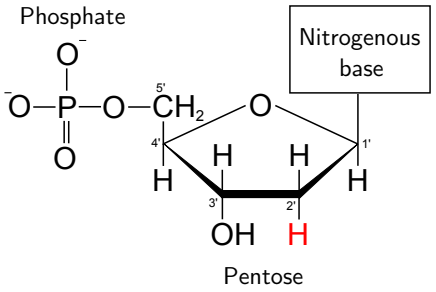

Figure 2.1. *Structure of the nucleotide. The pentose in the case of DNA is deoxy-D-ribose which is presented in the figure. In RNA the 2'-hydrogen is replaced by an OH-group making the pentose as D-ribose.*

polynucleotide chain of DNA consists of alternating sugar and phosphate groups. The ends of this chain are not identical. One (5') end contains a free phosphate group while an opposite one (3') a free hydroxyl group. Single-stranded (ss) polynucleotide chain has therefore directionality and a DNA-chain can be elongated in a living organism usually only to 3' direction by a DNA polymerase enzyme.

The third part of the nucleotide is an aromatic nitrogenous base which can be either a purine (adenine **A** or guanine **G**) or a pyrimidine (cytosine **C** or thymine **T**) in the case of a DNA molecule. In RNA, thymine is usually substituted by uracil (**U**) which differs from thymine by lacking a methyl group on its ring. The information of the polynucleotide chain is coded to the sequence of these particular bases. This sequence forms the primary structure of a polynucleotide chain. [1]

2.1.2 DNA double helix

Double-stranded DNA

Nucleotides form hydrogen bonds with each other via very specific arrangement in the base pairs. Purines form bonds with pyrimidines, with adenine bonding only to thymine and cytosine bonding only to guanine as stated in Chargaff's rules [2]. This is called complementary base pairing, and based on Chargaff's research Watson and Crick developed a model structure of DNA in 1953 [3]. Specific pairings have been presented in Figure 2.2.

Complementary strands can form a dual-stranded configuration called DNA double-helix. In fact, DNA is rarely existing in a single-stranded form in living organisms with two strands being separated only during the DNA replication process. Because of the complementarity, the two strands constituting the double-stranded DNA (dsDNA) run in opposite (3' to 5' and 5' to 3') directions within the helix. Thousands of relatively weak hydrogen bondings result in the very stable structure. Yet, the two strands can be separated for replication within energy scales similar to cellular metabolism.

Comparing AT and GC bondings together, we notice that GC bonding is stronger having hydrogen bonds between three pairs of atoms compared to the two bonds in AT pairing. Therefore the GC pairs contribute to the stability of DNA more than the AT ones.

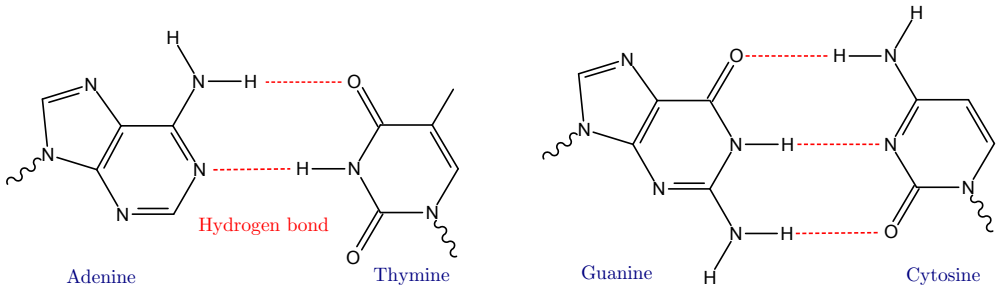

(a) (b)

Figure 2.2. Hydrogen bonds between A-T nucleotides (**a**) and G-C nucleotides (**b**).

DNA double-helix

The two strands composing a dsDNA form helical structure as a result of mainly two major types of interstrand interactions, namely the electrostatic repulsion and the attraction between strands. The low pK_a value of the phosphate group makes the dsDNA backbones negatively charged under physiological conditions (pH $\approx$ 7), and thus, the strands tend to repel each other. On the other hand, hydrophobic aromatic bases of the nucleotides attract each other by π-π -stacking effect, leading to attractive, non-covalent interactions between the aromatic rings. The energy values for stacking interactions and hydrogen bondings are correspondingly equal to 55-75 kJ/mol and 60-120 kJ/mol [4].

Depending on different factors, such as the sequence, chemical modifications of the bases and the environmental conditions, dsDNA can adopt different conformations namely A-, B- and Z- ones (Figure 2.3), B-form being the most common and stable conformation for a random-sequence under physiological conditions. These conformations are differentiated by the angle of the groove in relative to the main axis, width and the separation between the adjacent base pairs in the double-strand. For example, in B-DNA separation of two basepairs is 3.4 Å and the width of the double-strand is 22-26 Å [5]. The B- and Z-conformations have been directly observed in living organisms whereas A-DNA tends to form only under very dry conditions. [6]

2.1.3 G4-DNA

Some DNA forms are very different from the canonical Watson-Crick model. One of these structures is G4-DNA, which is formed by planar arrayed tetrads of hydrogen bonded G-bases, referred as G-guadruplexes, G-tetraplexes or G4-

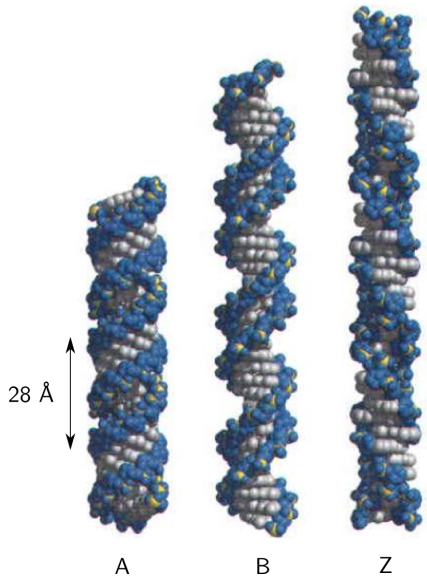

Figure 2.3. *Three most commonly referred conformations of dsDNA. Each structure has 36 basepairs. B- and Z-conformation can be observed in living organisms whereas A-conformation exists only under very dry unphysiological conditions. Note that in the Z form the helix is left-handed in contrast to right-handed helices of B- and A-forms. Image adapted from [1]*

DNA. The arrangement of hydrogen bonds is different compared to that in the Watson-Crick DNA. Each G base in the G4 tetrad forms hydrogen bonds with two neighbour bases via Hoogsteen bonding (Figure 2.4(a)). Planes of bases are further stabilized by monovalent cations, usually K^+ in the case of G4-DNA.

In the late 1980's synthetic G-rich single-stranded DNA were shown to form four-stranded structures. These structures have been studied further and it has been shown that G4-DNA may be formed by either one, two or four distinct strands of DNA depending on the length and amount of G-rich sequences within the DNA strands [7, 8]. Strands may be either parallel, antiparallel or a mix of both as shown in Figure 2.4(b) [9, 10].

Intramolecular G4-DNA structure may form when the sequence contains four distinct runs of at least three guanine bases in a relatively short (40-100 bases) oligonucleotide. Typical genomes in living cells contain plenty of such sequences. However, occurrence of G4-DNA in living cells is under discussion and they were long thought to be *in vitro* artefacts. Potassium concentration required to stabilize the G4-structures is in the scale of 10 mM, which is far below the typical concentration in mammal cells (120 mM). Also, proteins promoting formation and resolution of G4-structures have been identified in diverse organisms [11].

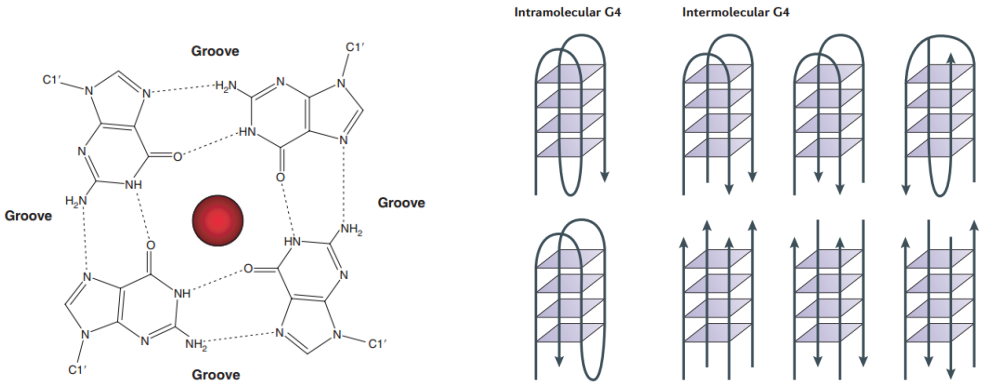

(a) (b)

Figure 2.4. Formation of the G4-DNA structure. Four guanine bases form tetrads arrayed in a plane via Hoogsteen hydrogen bonds, as shown in **a** [7]. Planes are stabilized by monovalent cations, especially potassium. Quadruplex structure may be formed by one, two or four distinct strands of DNA depending on the sequences of nucleotides. In **b** is shown some of the simplest ways of folding [7].

Computational studies have shown that G4 motifs, sequences possible to form guadruplex structures, are not randomly located in the chromosomes. Furthermore, such motifs are clearly conserved among related species. These facts indicate that G4 structures may have significant roles in the cellular functions. It has been also proposed that they may be targets for some regulatory enzymes used for gene expression. G-guadruplex structures also directly suppress DNA transcription so that cells have been forced to evolve mechanisms to unwind the structures. Interesting fact is that the G4 forming sequences have been reported to occur within the regulatory regions of several oncogenes (genes potential to cause cancer) [12, 13], which would make them potential targets for therapeutic molecules. In addition, many telomeric sequences of linear mammalian chromosomes fold into tetraplexic structures, which may indicate that the formation of the G-guadruplexes plays a role in cells ageing processes [14].

2.1.4 Synthetic fabrication methods

Relatively short oligonucleotides, i.e. under 100 nucleotides, with specific sequences are easy to fabricate from single nucleotides using chemical synthesis. There are several synthetic pathways available, reviewed in reference [15]. Error frequency increases with longer oligonucleotides, which limits the length of the

synthesized DNA usually to under 100 nucleotides, although artificial genes with thousands of base pairs have been synthesized [16]. Synthesized DNA strands may further be modified by chemical synthesis, e.g., adding functional groups to them.

2.2 Applications of DNA self-assembly and metal-nanoparticles

2.2.1 DNA sticky ends and branched DNA

DNA is especially suitable for bottom-up fabrication of different kinds of nano- and even microstructures because of its dimensions and superior self-assemble properties. Simplest way to utilize the properties of DNA is to introduce so called 'sticky ends' to both ends of a dsDNA. Sticky ends are short single-stranded overhangs in the ends of a double-stranded structure, routinely used in the methods of molecular biology [17]. Two complementary sticky ends may be linked together via hydrogen bonds creating longer contiguous chains of dsDNA. This property may be used further to make 1D structures, such as chains or rings [18].

It is possible to fabricate more complex structures by introducing branched junctions consisting of three to eight distinct ssDNA strands. This method was introduced by Seeman *et al* [19]. These junctions of DNAs may further be used to create, e.g., 2D planes of periodic structures [20].

2.2.2 DNA-origami structures

By utilizing the self-assembly properties of DNA strands one can create complex 2D and even 3D structures also by so-called origami technique, which was introduced rather recently (Rothemund, 2006 [21]). In this technique a long (7000-9000 nucleotides) single-stranded DNA strand, which acts as a scaffold for the final structure, is folded into a wanted form with the help of so-called staple oligonucleotides, which are programmed to fit into specific locations in the structure. In principle the scaffold strand can be any ssDNA which is long enough to fill the space required for the desired shape, as long as the sequence does not have too many recurring or complementary sequences.

Each shape of origami requires very specific staple strands (typically about 200 different strands is used for about 100 nm origamis). Ideally each staple should be able to hybridize between only two specific motifs in the scaffold

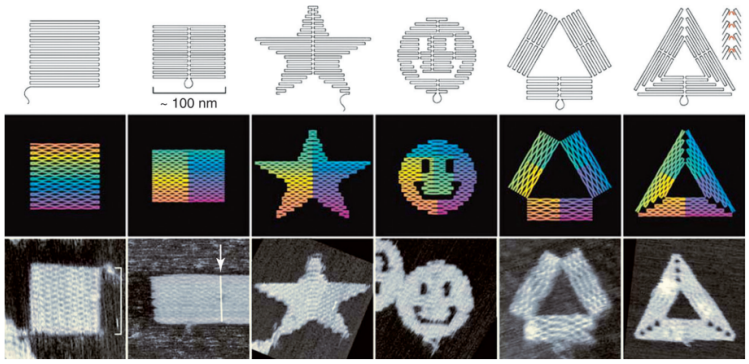

Figure 2.5. *Schematic drawings (upper rows) of some fabricated 2D DNA origami structures and their AFM images (lowest row) [22]. Top row represents the folding of the scaffold strand only. In the middle row staple strands have been added. AFM images in the bottom row correspond to a size of* $165 \times 165\,\mathrm{nm}^2$. As the pictures demonstrate, the shapes of the final products are well defined and therefore the structures are rigid.

strand. Therefore, the design has to be made with the help of custom-made computer programs. Some 2D DNA origami designs have been presented in Fig. 2.5. Technique has been further extended for fabrication of 3D structures which opens up almost limitless possibilities to create different nanodevices [23]. In practise, the whole process is so-called 'one pot'-process and the assembly of the structures happens in a single step which makes the method relatively easy, low-cost and potentially suitable for mass production.

Bare origami structures may seem to be just a curiosity. However, basically each staple strand can be functionalized separately by attaching chemical groups or even whole nanostructures to them, which increases the uses of this technique tremendously. Functional groups can be added with the resolution of about 6 nm which enables fairly complex patterns.

2.2.3 Metal-nanoparticles

Metal-nanoparticles have already been proven to be highly useful in many applications in optics, catalysis, electronics and many other areas [24, 25, 26, 27] due to their unique size-depended properties. Especially noble metal-nanoparticles have gained much interest. The properties of these particles with dimensions less than 100 nm differ tremendously compared to the corresponding bulk counterparts typically because the surface area of nanoparticles per weight is much greater than in larger particles. The size-dependent properties have been possible to be exploited only rather recently since the synthetic methods have

not been evolved enough until now. Nowadays it is possible to tailor the sizes, shapes of metal-nanoparticles in a controllable way [28].

The mean free path of noble metals is in the order of 50 nm [29], which means that in particles smaller than this no scattering of electrons is expected. Thus, all interactions are expected to be with the surface. Rather recent observation is, that on the surface the electrons oscillate collectively in the conduction band. In metal-nanoparticles the oscillation frequency corresponds typically to wavelengths in the region of the visible and near-infrared light. This feature gives noble metal-nanoparticles typical optical properties due to strong surface plasmon resonance (SPR) absorption, which can be tuned suitably by modifying the dimensions of the particles. Tunability of the absorbance characteristics makes metal-nanoparticles very exploitable for sensing and imaging techniques [30].

SPR sensors are divided into two types depending on the operation principles. The resonance conditions required to excite the surface plasmons depend on the environment of the metal surface, more accurately the refractive index of the medium next to the surface. Changes in the refractive index may be caused for example by binding of other molecules. Sensors based on this type of operation are already commercially available [31]. Second kind of sensors are based on the fact that plasmons are able to couple at short distances thus shifting the SPR conditions [32].

Silver nanoparticles

Silver-nanoparticles (AgNPs) are used nowadays commercially as antibacterial agents in a wide range of applications such as water treatment, textile manufacturing and bioengineering. Already since the 18th century silver nanoparticles have been used e.g. in treatment of ulcers and burn wounds [33]. Other possible future applications of silver nanoparticles include high-sensitive nanoscale sensors [34], catalytic agents [35, 36] and optical applications such as new types of optical data storage [37], biological labels and electroluminescent displays [38].

Gold nanoparticles

Suitably tuned gold nanoparticles (AuNPs) possess near-infrared absorptive spectral properties, making them active in the so called 'biological window'. Biological window defines the range of wavelengths which have the deepest penetration into biological tissues, thus AuNPs can be used in many medical applications. Indeed, many applications have been introduced, including usage

of AuNPs as photothermal therapy agents [39] and components for biodetection and diagnostics [28, 40] based on the optical properties of them. AuNPs are also very efficient catalytic agents [41].

2.2.4 DNA-metal-nanoparticle conjugates

Overlap between molecular biology and nanosciences is nowadays evident. It is possible to create nanodevices which utilize the unique characteristics of different biological molecules and combine them to the properties of nanoscale objects [42]. Again, programmable properties of DNA makes it arguably one of the most useful tools to assemble nanostructures in a highly controllable way. For example functionalizing nanoparticles by a layer of single-stranded DNA allows the conjugates bind specifically to molecules, such as proteins or other biomolecules, functionalized with a complementary sequence. These kind of modifications are very promising candidates for the future drug design [28, 39]. By utilizing self-assembly properties of DNA one can also fabricate complex functional metamaterials, i.e. artificial periodic materials that do not occur in nature, based on the SPR properties of metal-nanoparticles. The resolution of earlier fabrication methods, such as lithographic techniques, have been limited and the fabrication has been challenging. However, DNA-directed self-assembly offers methods to create structures with extraordinary resolution and is therefore very promising tool in this field of research. Applications have already emerged [43].

Establishing a covalent connection between DNA strand and a metal-nanoparticle is possible by functionalizing the free ends of the oligonucleotides with ionizable groups, such as thiol-groups (-SH). This was first demonstrated by Alivisatos and Mirkin in 1996 [44], who conjugated DNA with gold nanoparticles. Since then these kind of modifications have been exploited widely. However, one of the issues functionalizing nanoparticles with DNA is that DNA strands are known to adsorb also non-specifically on the surface of metal nanoparticles [45] depending on the oligonucleotide content, oligonucleotide length, rigidity and coverage. In order to prevent this, various methods have been introduced [46].

2.3 Electrical conductivity of DNA

The idea of using DNA molecule as a conductive wire was originally proposed in 1962 by Eley and Spivey who made measurements with four different DNA

samples and one RNA sample pressed in between of two platinum electrodes [47]. It was proposed that charge carriers moving along DNA strands play an important role in the repair mechanisms of DNA. The results obtained by Eley and Spivey were quite constant between the samples; specific resistance was about $5 \cdot 10^{-11}\,\Omega$cm at 400 K with an energy gap of 2.42 ± 0.05 eV. They concluded from the results that π-stacked electronic structure of the bases served as the main conduction channel for the charge carriers. Since then the conductance properties of a DNA strand have been under vigorous research. The results obtained by different research groups have varied greatly. The challenge is that the electron transfer through the DNA is strongly depended on the conformation of the polymer. Hence, the sequence of the strand and the environment conditions have major affect on the conductivity. [48]

Many kinds of experimental methods have been introduced for the determination of the conductance properties of DNA. These can be divided into the two main types of approaches: direct and indirect measurements. Utilizing nanomanipulation methods makes it possible to introduce DNA strands, even a single strand, in between two electrodes [49]. Applying voltage between the electrodes the corresponding current can be measured and the conductivity of the sample be determined. These kind of measurements represent direct approaches. Alternative approach is to use indirect methods in which a solution of DNA strands is examined by the means of spectroscopic measurements. However, it is important to emphasize that these measurements offer very different kind of information about the properties of DNA. In the next two sections we will touch upon this issue.

2.3.1 Charge transfer, indirect measurements

In the earlier measurements on DNA, indirect methods were used. The main idea of this indirect approach is to introduce a charge donor and acceptor in the different ends of the strands as part of the DNA helix. Donor and acceptor may be e.g. molecules containing similar aromatic groups as the bases of nucleotides, which enables them to intercalate either partially or fully inside the DNA strand. They may also be molecules covalently bonded to the DNA strand or modified nucleotides or specific sequences. Either way, electromagnetic radiation is used to release a photoelectron from the donor, which is migrated assumingly along the DNA strand to the acceptor. This oxidation-reduction reaction can be observed by the means of steady-state spectroscopic methods as a decay of the excitation state of the acceptor.

A simple way of modelling charge transfer (CT) through a one-dimensional potential barrier, such as a set of π-stacked nucleotides, was introduced by A. Marcus [50]. His theory states that the CT efficiency k_{CT} (the rate of tunneling events) is simply

$$k_{CT} = k_0 e^{-\beta D}, \tag{2.1}$$

where k_0 is the rate of the CT when acceptor and donor are in immediate contact, D is the distance travelled by the charge carrier and β is coefficient describing the cohesion of the electronic orbitals between molecules. Therefore, β describes how fast the tunnelling rate is falling off as the function of the distance. Theoretically it was proposed that the value of β is in the case of DNA strand in the range of $0.85\,\text{Å}^{-1}$-$2.5\,\text{Å}^{-1}$ [51].

One of the most influential indirect measurements have been made by Barton *et al.* Their results have varied from insulator-like ($\beta \approx 1\,\text{Å}^{-1}$) to ohmic, high conductive behaviour ($\beta \approx 0.1\,\text{Å}^{-1}$) [52, 53]. A number of different intercalators were used, which could, at least partly, explain the differences between the experiments. Therefore, different extents of interactions between the reactants and DNA base stack should be considered carefully [54].

Wide range of results induced active discussion about possible mechanisms of CT in DNA strands. It was getting evident that the sequence of the DNA strand under investigation plays a major role on the mechanism and efficiency of CT [55]. In 1998 Meggers *et al.* made an experiment in which a radical cation $G^{+\bullet}$ and base triplet GGG, separated by one to four AT base pairs, were used as charge donor and acceptor respectively [56]. CT efficiency was reduced one order of magnitude when one AT pair was introduced in between the reactants and value of $\beta \approx 0.7\,\text{Å}^{-1}$ was obtained. However, if the second or the third AT pair of the four pairs was exchanged to a GC pair, the CT rate was increased by two orders of magnitude. CT of a strand containing 15 mixed base pairs was also determined. The results indicated that the CT could be described as a hopping of the charge carriers between only the intervening G bases, characterized by the lowest oxidation potential amongst the DNA nucleotides.

The above described, so-called G-hopping CT mechanism does not apply in the sequences containing long (>3 bp) tracts. The results obtained by Giese *et al.* [57] indicate that there is also another CT mechanism in which AT base pairs have a major contribution to the CT. The DNA strand was equivalent to the DNA used by Meggers *et al* ($G^{+\bullet}(AT)_nGGG$, n = 1-16). From the results (presented in Fig. 2.6) two different processes can be clearly differentiated: CT efficiency over short (n = 1-3) AT tracts is characterized by a rapid decrease

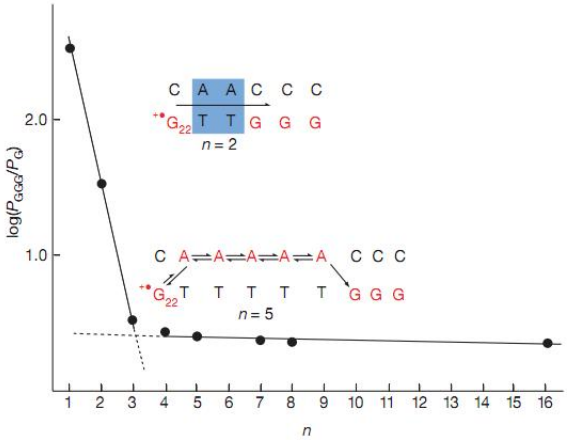

Figure 2.6. Results obtained by Giese *et al* [57]. Determined value of $\log P_{GGG}/P_G$, describing the charge transfer rate, has been plotted. P_G describes the strand cleavage product after piperidine treatment of the sample whereas P_{GGG} is the water trapping product. The ratio P_{GGG}/P_G was determined by gel electrophoresis using assay described in [58]. Synthesised DNA strand was $G^{+\bullet}(AT)_nGGG$, in which n was varied between 1-16. For small values of n (< 4) CT is characterized by a strongly distance-dependent tunnelling process between G bases, whereas for longer distances CT efficiency is only slightly influenced by the number of AT base pairs. CT over long AT tracts can therefore be described by thermally induced A-hopping mechanism.

as the function of distance, indicating G-hopping mechanism described earlier, whereas for longer distances CT efficiency is only slightly influenced by the number of intervening AT base pairs. Mechanism can be explained by the time scales involved in the reduction-oxidation processes of the bases, i.e. A-bases may oxidize significantly if the time constant of the G-hopping reaction exceeds the time constant of adenine oxidation reaction. In this case the charge migrates via multi-step process, referred by A-hopping mechanism.

Temperature-dependence of the A-hopping mechanism was further studied by O'Neill & Barton [59]. The CT efficiency increased linearly as the function of temperature between temperatures 0-60 °C (presented in Fig. 2.7(a)), which remarks the role of thermally activated A-hopping reactions. More interestingly, certain number of AT base pairs seemed to be more favourable for the CT as an oscillatory component, with a period of 4-5 base pairs, was evident (Fig. 2.7(b)). This indicates that the distance dependency of CT efficiency along the DNA strand does not exhibit a single function. Hence, the distance dependence of the CT was no longer characterized by the constant β in the case of long random-sequenced DNA strand, typically containing long AT-tracts in between successive G-bases. Every intervening base has an effect on the configuration

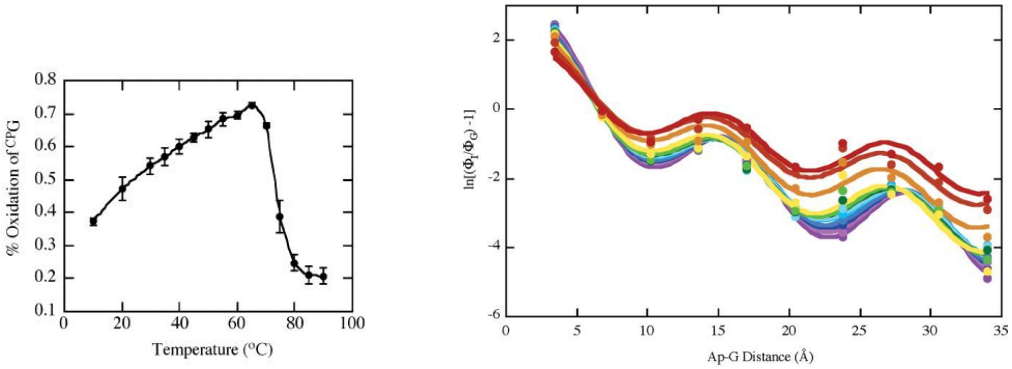

(a) (b)

Figure 2.7. *Results obtained by O'Neill & Barton [59]. In (**a**) is presented the relative oxidative damage induced by Ap* (photoexcited 2-aminopurine) in the DNA duplex ApAAAG. Data points represent averaged values of three individual measurements. The dependency is rather linear in temperatures below* $60\,^{\circ}\mathrm{C}$*, until the yield of damage decreases dramatically as the DNA strands separate. In (**b**) the yield of CT is presented as the function of distance in the temperature range of* $0 - 55\,^{\circ}\mathrm{C}$ *(increasing from violet to red). Shown is a plot of* $ln[\Phi_I/\Phi_G - 1]$*, in which* ϕ *represents fluorescence intensity, versus Ap-G distance.*

of the whole structure, so it is understandable that certain base configurations have higher probability of accessing CT-active conformations.

In conclusion, simple model for CT efficiency along DNA strand can not be formulated and the parameter β is not usable in the case of long, random-sequenced DNA. However, there is a consensus that G bases are responsible for the charge transfer if the intervening AT-tracts are 'short' (1-3 base pairs). The results obtained from indirect measurements have demonstrated that carefully selected DNA may have good charge transfer capabilities, which is very encouraging in respect of DNA-based molecular electronics. Moreover, information about the charge transfer mechanisms have been obtained, which has a great relevance for biological aspect, as the DNA-mediated charge transfer has great relationship to the DNA damage and repair systems [60].

2.3.2 Electronic conductivity, direct measurements

Electronic conductivity

When the transport of charge carriers is dominated by scattering events, conductivity of the material is described by Ohm's law

$$J = \sigma E, \tag{2.2}$$

where J is the current density at a given location in a resistive material, E is the electric field at that location and σ is a material dependent conductivity. Usually Ohm's law is expressed in a macroscopic form $U = RI$, where U is the applied voltage, R is the resistance of the material and I is the current through the conductor. Resistance is dependent on the properties of the material as well as its dimensions. The resistance for a given material is inversely proportional to the cross-sectional area and directly proportional to the length l. Therefore resistance can be calculated as

$$R = \rho \frac{l}{A}, \tag{2.3}$$

where ρ is material dependent electrical resistivity (also called specific electrical resistance). Reciprocal of resistance is called conductivity $G = \frac{1}{R} = \sigma \frac{A}{l}$, where σ is the electrical conductivity. It has to be noted that Formula 2.3 is only an approximation in practical situations, as the current density has to be assumed uniform in the conductor.

If the mean free path of the charge carriers (the average distance travelled by the charge carrier before a single scattering event) is much bigger compared to the size of the material, which limits the path of the charge carrier, ballistic transport is observed. This is typical for nanoscale objects such as nanowires and molecules through which charge carriers can pass from one end to the other without being scattered at all. In the case of the ballistic transport Ohm's law is not valid and the concept of electrical resistance is different.

In the following a quasi one-dimensional wire with diameter much smaller than the mean free path is considered as presented in [61]. Along the wire the electron eigenstates carrying the electric current (in the z-direction) are Bloch-waves with quantized energy bands (subbands). For free electrons the energy of each subband is

$$E_i = \epsilon_i(k_x, k_y) + \frac{\hbar^2 k_z^2}{2m^*}, \tag{2.4}$$

in which ϵ_i are the discrete energy levels resulting from the k_x, k_y-quantization, k_x, k_y and k_z the components of the k-vector and m^* the effective mass of the

state. The wire is assumed to have a rectangular cross section. Current carried by each subband from one electron reservoir to another is to be calculated. Now the difference between the chemical potentials of left and right reservoir as the function of the voltage U between the contacts is

$$\mu_L - \mu_R = eU. \tag{2.5}$$

The current in one subband, when only the electron states between μ_L and μ_R contribute to the current flow, is

$$I_i = e \int_{\mu_R}^{\mu_L} D_i(E) v_i(E) \mathrm{d}E, \tag{2.6}$$

in which $v_i(E)$ is the group velocity of electrons in the subband i and $D_i(E)$ the one-dimensional density of states in the subband i. The group velocity is given by

$$v_i(E) = \frac{1}{\hbar} \frac{\partial E_i}{\partial k_z} \tag{2.7}$$

and the density of states in one-dimensional case

$$D_i(E) = \frac{2}{h v_i(E)}. \tag{2.8}$$

Inserting previous equations to 2.5 gives

$$I_i = \frac{2e^2}{h} U. \tag{2.9}$$

In the case of ballistic transport each subband therefore carries the same current with the universal conductance

$$G_0 = \frac{2e^2}{h} = 7.748\ldots \cdot 10^{-5}\,\Omega^{-1} \approx \frac{1}{129\,\mathrm{k}\Omega}. \tag{2.10}$$

Taking into account a so-called transmission coefficient of the channel T, describing the probability of a particle tunnelling through a barrier, the conductance is

$$G = G_0 T = \frac{2e^2}{h} T. \tag{2.11}$$

The total conduction of the sample is therefore dependent on the number of available charge carrying subbands and can be written as

$$G(\mu) = G_0 \sum_n T_n(\mu), \tag{2.12}$$

which is called Landauer formula.

Earlier direct conductivity measurements

Encouraging experimental data from the indirect measurements, suggesting high CT rates in DNA molecules, induced a series of direct conductivity measurements as soon as the technology in the field of electron beam lithography and atomic force microscopy was advanced enough. However, the direct conductivity measurements of DNA have turned out to be a very challenging topic of research as the experiments have reported very wide range of electronic properties. While indirect experiments seemed to converge on a general understanding of DNA CT properties, the results of direct measurements have varied from insulating, semiconducting and conducting, even superconducting, behaviour of DNA [48, 62]. However, several reasons for the contradicting results can be assorted.

One of the first direct measurements indicating ohmic, low resistance behaviour of DNA, was published in 1999 by Fink *et al.* who reported high electrical conductance of bacterial-origin random sequenced λ-DNA bundles [63]. In the experiment they used modified LEEPS (Low Energy Electron Point-Source) microscope for locating the sample which was laid across 2 µm holes in Au-coated carbon foil. Au-coated mechanical tip was positioned in contact to a single DNA bundle and voltage between the tip and the foil was applied. However, it was later proved by De Pablo *et al.* that low energy electron beam may induce observed conductance by either doping the DNA or accumulating a contamination layer around the DNA strands [64]. The group measured the resistance of a λ-DNA deposited on an insulating mica surface. DNA was connected to a gold electrode, which was evaporated on the surface on top of the end of the DNA. An Au-coated AFM tip was used as a second electrode connecting to the DNA. Applying bias voltage of up to $\pm 10\,\mathrm{V}$ they detected no trace of current going through the DNA.

One problem with this kind of set-up is evident: the contacts of DNA π-electron stack to the AFM tip and the gold electrode. Evaporating a gold layer on DNA might alter the electronic structure and the configuration of the DNA. However, as indirect measurements had pointed out, it was evident that random-sequenced dsDNA was a poor conductor. On the other hand, Kasumov *et al.* emphasized the importance of the substrate in direct conductance measurements for DNA [65]. If the DNA is in direct contact with the substrate, strong interactions may induce very large conformal deformation of the deposited DNA. This was proven by using two different substrates: bare and NH_3^+ covered mica. On bare negative charged mica the typical height of

λ-DNA duplex was shown to be 1 nm. If the charge of mica is cancelled out by positive NH_3^+ ions, the diameter was of the order of 2 nm, close to the native conformation of B-DNA. On bare substrate DNA strands were insulating, whereas on treated substrate the resistance was dropped to only 55 kΩ. The contribution of ionic conduction did not explain the results as the strands were conductive also in cryogenic temperatures. Also kinks and bends were shown to decrease conductivity significantly. These results emphasize the importance of DNA conformation for the charge transfer capability.

In 2000, Porath *et al.* trapped 10.4 nm long poly(G)-poly(C) DNA molecules in between two metal nanoelectrodes with 8 nm gap [66]. The measurements were carried out in both air and vacuum down to cryogenic temperatures. They obtained non-linear current-voltage curves indicating semiconductive behaviour with a large 1.5-2.0 volt band gap. However, in this experiment the DNA strand did not establish covalent bonds with the metal electrodes, which most likely explains the poor conductivity. This problem was solved in 2003 by Bhattacharya *et al.* who introduced a technique to anchor DNA strand covalently to metal nanoelectrodes by using free thiolate groups (-SH) in both ends of G-rich dsDNA [67]. Results did not indicate any band gap due to the well-defined bonds between the electrodes and DNA, although I-V curves were non-linear. The measured maximum currents were in the range of 2-400 nA using bias voltages up to 1 V which was a significant increase compared to the results obtained earlier.

Various studies have shown that increasing the relative humidity of the environment increases the conductivity of DNA in direct measurements [68, 69, 70]. This can be explained at least by two ways. Water may gather around DNA strand forming a hydration layer which acts as a pathway for ionic conductivity [71]. On the other hand, as the conformation of DNA is highly affected by the conditions of the environment, the π-stacking of the bases is more suitable for electronic condition at high humidities compared to the dry form of DNA [49, 71, 72].

Xu *et al.* were able to eliminate the effects of molecular contacts and the conformations of DNA in their experiment in 2004 [73]. All the measurements were done in an aqueous solution in order to keep the dsDNA molecules in their natural B-conformation. Individual molecular junctions were created by repeatedly moving an AFM tip into and out of contact with a flat Au electrode in the buffer containing the sample DNA as shown in Figure 2.8(a). The tip was insulated over the most of its surface to eliminate any leakage currents. Two sets

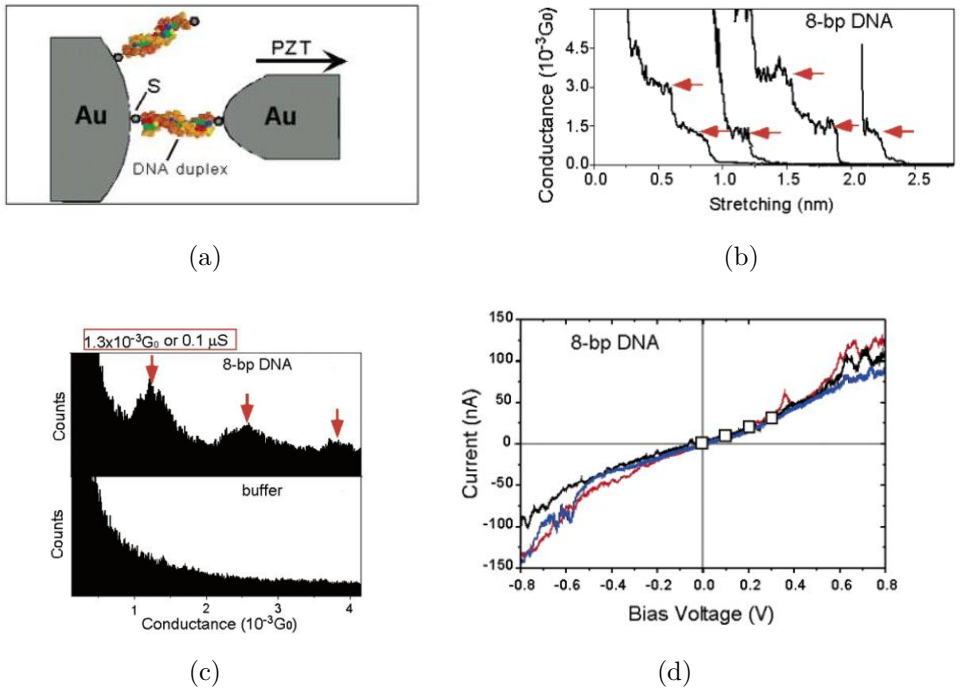

Figure 2.8. *Measurements performed by Xu* et al. *(**a**) Schematic illustration of a single DNA conductance measurement. (**b**) Discrete steps in the conductance form due to formation and breakdown of individual molecules in the case of 8-bp GC DNA duplex. (**c**) Conductance histogram constructed from more than 500 individual measurements. Well-defined peaks are shown near-integer multiples of a fundamental value of* $1.3 \cdot 10^{-3} G_0$*, corresponding to the conductance of a single DNA duplex (8-bp GC sequence). (**d**) Three different current-voltage curves of a single eight-bp DNA showing linear behaviour up to voltages of* $\pm 0.5\,\mathrm{V}$.

of thiol-modified sequences were used: 5'-$(GC)_n$-3' and 5'-$CGCG(AT)_m CGCG$-3' with $n = 4$, 5, 6, and 7 and $m = 0$, 1, and 2. Therefore, the length dependence of conduction could be determined.

Conductance G as the function of r (the distance between the tip and the surface) was determined over 500 times for all of the samples (Fig. 2.8(b)). As can be seen, a series of steps appear in the conductance. These steps did not always appear at the same conductance values, due to variations in the conformations of the DNA strands and the molecule electrode contacts. The variations were averaged out by constructing a histogram shown in Figure 2.8(c). The histograms revealed well-defined individual peaks near-integer multiples due to the contact of individual molecules. In the case of 8-bp GC sequence the multiple is $1.3 \cdot 10^{-3} G_0 \approx 0.1\,\mu\mathrm{S}$ corresponding to the conductance of a single DNA duplex. Ultimately, length dependency of conductance was determined,

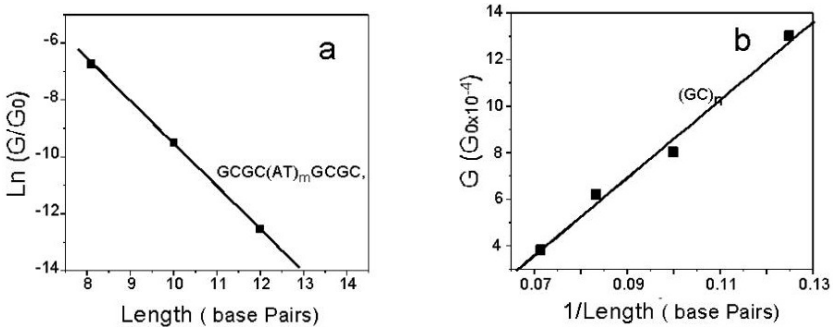

(a) (b)

Figure 2.9. *Results obtained by Xu* et al. *[73] revealing two different length dependencies of conductance. In (***a***) natural logarithm of $(AT)_m$ DNA conductance vs length is plotted showing exponential decay of conductance. The decay constant β can be determined from the slope of the linear fit. In (***b***) conductance of $(GC)_n$ DNA is plotted vs 1/length. In this case the length dependency is $G = a \cdot \frac{1}{r}$.*

shown in Figure 2.9 revealing different behaviour of two series of samples. The conductance for the $(GC)_n$ sequence was proportional to the inverse of length $1/L$ whereas for 5'-CGCG$(AT)_m$CGCG-3' sequence the decrease in conduction was exponential with a decay constant of $\beta \approx 0.43\,\text{Å}^{-1}$. Also alternative method was used to determine I-V curves. The method started by pulling the tip out of contact with the Au-electrode until the distance corresponding to the lowest conductance plateau. The tip was frozen and the I-V characteristics were measured by sweeping the bias voltage (Fig. 2.8(d)) showing rather linear behaviour up to voltages of $\pm 0.5\,\text{V}$. The results highlight that the conductance of DNA is strongly sequence-dependent also in direct measurement.

Rather recently direct conductance measurements have been made also for alternative conformations of DNA, such as G4-DNA. Due to the high guanine content and surface area in each tetrad, it has been proposed that the improved overlapping of π-stack p-orbitals make the CT properties of G4 structures superior compared to the regular DNA. Also G4-wires have revealed considerable stability in various conditions [74, 75], which would make them ideal molecular wires for many applications.

Only few direct conductance measurements have been made for G4-wires. The conductivity and the structural stability of G4-wires was demonstrated by Liu *et al* [76]. To measure G-quadruplexes they used a mechanically controlled break juction (MCBJ) experiment. The G-quadruplexes were thiol-modified in order to establish a covalent coupling of the molecules to gold electrodes

of the MCBJ. Resistance as a function of distance r (length of the MCBJ) was recorded showing plateaus in resistance with length in the order of 2 nm upon shortening and lengthening the distance. Depending on the sample, this behaviour was reproducible for about 30 repetitions until the plateau vanished. The resistance of the plateaus were in the order of $10^8\,\Omega$. The resistance of a single G4-wire was therefore found to be independent of the stretching of the structure. Moreover, the conformation of the sample DNA was highly reversible. These results indicate that G4-wires would make an interesting candidate for nanoelectronic applications.

3 Materials and experimental methods

3.1 Fabrication of DNA-coated metal-nanoparticles

3.1.1 Silver-nanoparticles

Colloidal silver nanoparticles (AgNPs) with a diameter of 20 nm were prepared in an aqueous solution by the reduction of $AgNO_3$ in the presence of borohydride ($NaBH_4$) as follows. A volume of 180 mL deinoized and filtered water was precooled to 4 °C. 0.45 mL of freshly prepared 0.1 M $AgNO_3$ solution was added under vigorous stirring. Subsequently 0.90 mL of 50 mM (tri)sodium citrate and 0.75 mL freshly prepared 0.6 M $NaBH_4$ solution was added under vigorous stirring. Here $NaBH_4$ acts as a reducing agent and sodium citrate stabilizes the formed particles. The vigorous stirring during mixing the solutions is crucial for producing uniform particles. Once the $NaBH_4$ solution was added the mixture was turned clear yellow immediately. The solution was left at 4 °C for over night after which it developed a dark yellow colour. To further stabilize the particles, 0.72 mL of 2.5 M LiCl was added under vigorously stirring. Subsequently, solution was transferred into 13 mL DuPont pyrex tube and centrifuged at 11,000 rpm for 45 minutes at 20 °C in Sorval SS-34 Rotor. Clear supernatant was carefully removed and a fluffy pellet was collected and suspended in 4 mL of residual supernatant. The UV-Vis spectrum of the suspension was measured with UV-Vis spectrophotometer and optical density (OD) of around 100 at 400 nm was obtained. The concentration of the particles is given by Beer-Lambert law

$$A = \epsilon \cdot l \cdot c, \tag{3.1}$$

in which A is the absorbance, ϵ the extinction coefficient ($3 \cdot 10^9\,\mathrm{M^{-1}cm^{-1}}$ in the case of 20 nm AgNPs [77]), l the optical path length and c the concentration of the sample.

3.1.2 Gold-nanoparticles

20 nm *particles*

In this protocol 20 nm Au-nanoparticles were synthesized by reducing gold ions in aqueous solution. Synthesis begun by preheating 100 mL double-distilled and filtered water to the boiling point. Water was poured in the boiling kettle and it was heated in an oil bed. Heater was equipped with a magnetic stirrer which was kept on for the whole time of the procedure. Boiling kettle was connected to a water cooling system in order to prevent losses of water used for the actual synthesis. 1 mL 0.12 M $HAuCl_4$-solution was added to the boiling water. 10 mL 38.8 mM sodium citrate was added subsequently for the reducing reaction. At this point the stirring of the water was crucial in order to produce uniform nanoparticles. Approximately 5 minutes after addition of the reducing agent the colour of the solution was changed to dark red because of the plasmonic effect in formed nanoparticles consisting of several hundreds of gold atoms. The solution was incubated for 15 minutes at the boiling point after which the solution was cooled to room temperature and stored.

The absorption spectrum of the prepared solution was measured with a UV/Vis spectrophotometer in 0.4 cm optical path quartz cuvette revealing OD at 520 nm peak of around 3.0. The concentration was increased by centrifuging in a Sorval SS-34 Rotor at 10,000 rpm and 17 °C for 15 minutes, after which the absorption spectrum was again measured and OD of 50 was obtained (at 520 nm) corresponding to a concentration of around 120 nM using an extinction coefficient $\epsilon = 4.2 \cdot 10^8\,\mathrm{M^{-1}cm^{-1}}$ [78].

60 nm *particles*

AuNPs with a diameter of 40-60 nm were prepared using a modified version of the protocol used for preparing the smaller AuNPs described above. Again, 100 mL double-distilled water was heated to the boiling point and 1 mL 0.12 M $HAuCl_4$-solution was added. After this, 420 µL of 38.8 mM sodium citrate was added to the mixture. The solution turned dark and subsequently purple approximately after 5 minutes. The mixture was incubated under boiling conditions for 15 minutes and cooled down to the room temperature. The absorption spectrum was measured and OD at 525 nm of around 1 was obtained. The mixture was concentrated by centrifuging at 3,000 rpm for 8 minutes in a Sorval SS-34 Rotor. A clear supernatant was carefully discarded and the pellet was collected. UV-Vis absorption spectrum revealed an OD of around 150 at 525 nm.

The extinction coefficient of colloidal gold-nanoparticles with specific diameters can be calculated using formula

$$\epsilon_{\text{particles}} = \mathrm{e}^{k\ln D + a}, \tag{3.2}$$

where parameters $k = 3.3214$ and $a = 10.805$ are experimentally obtained and D is the diameter of the particles in nanometers [79]. Plugging in the average diameter $D = 50\,\text{nm}$ one obtains $\epsilon = 2.2 \cdot 10^{10}\,\text{M}^{-1}\text{cm}^{-1}$

3.1.3 G4-DNA strands

In this procedure short (10-30 bases) oligonucleotides $\text{a}_5^*\text{G}_{10/30}\text{a}_5^*$, where a^* represents phosphorotioated adenine and G regular guanine nucleotide, were used for synthesis of G4 structures.

Dissolving of the oligonucleotides

The procedure begun by dissolving oligonucleotides (6786 µg, 1.07 µmol, purchased from Alpha DNA, Montreal, Canada) to 0.2 mL volume of 0.1 M LiOH after which the solution was incubated for 5 minutes at room temperature and centrifuged for 2 minutes at 14,000 rpm with Lumitron *eppendorf 5418* centrifuge . The clear supernatant was collected and the absorption spectrum was measured using 1 cm quartz cuvette with UV/Vis spectrophotometer revealing OD 400 at 260 nm.

Size-exclusion chromatography

The oligonucleotide solution was separated from the low molecular weight components present in the buffer solution on a Sephadex *G-25 391197 GE Healthcare* DNA-grade column (Amersham Biosciences) equilibrated with 2 mM Tris-Ac (pH 8.5). The oligonucleotide was loaded in 500 µL and eluted in ~ 0.5 mL of 0.1 M LiOH. Then 200 µL of 2 mM Tris−Ac (pH 8.5) was added and the collection was started. The sample was collected in ~ 700 µL. Concentrations of the nucleotides were calculated using absorption coefficient of $976\,\text{mM}^{-1}\text{cm}^{-1}$ and $1696\,\text{mM}^{-1}\text{cm}^{-1}$ for G_{10} and G_{30} respectively.

Formation of G4-structures

Folding of the eluted G-strands into G4-structures was induced by adding 67 µL 1 M Tris-Ac (pH 8.5) to the final concentration of 100 mM. The sample was incubated for 30 minutes at room temperature and passed through Sephadex

G25 column as shown above. The only difference is that now the column was equilibrated with 15 mM Na-Pi (pH 8.0).

3.1.4 Preparing the metal-nanoparticle-DNA conjugates

20 nm *AgNP dimers bridged with G4-DNA*

A 4 mL fraction of AgNP-Cl solution, prepared as described in section 3.1.1, was incubated with the presence of 10 μM $A_{10}a_5^*$ oligonucleotide solution. The mixture was incubated for 1 hour at room temperature. Subsequently, 1 M NaCl was added to final concentration of 25 mM and the mixture was incubated for 1 hour at 50 °C and loaded onto a Sepharose 6B-CL column equilibrated with 10 mM Na−Pi buffer (pH 7.4) at a flow rate of 0.6 mL/min. The particles were eluted with 40-50 mL of the buffer and were completely separated from non-bound oligonucleotides. The particle-DNA conjugates were concentrated by centrifugation at 14, 000 rpm in room temperature for 25 minutes on Eppendorf *Table 5424* centrifuge. The concentration of the particles was calculated using an extinction coefficient $\epsilon = 3 \cdot 10^9\,\mathrm{M^{-1}cm^{-1}}$ at 390 nm [80]. It has been shown, described in [81], that mixing silver-nanoparticles, coated with 15-mer adenosine oligonucleotides, with G4-DNA flanked with phosphorotioated adenosine nucleotides, leads to formation of conjugates consisting of discrete number of the nanoparticles bridged with G4 structures. The conjugates can be purified using gel electrophoresis as described in section 3.1.5. Clear bands containing these chains of AgNPs has been presented in Fig. 3.1(b). TEM images of chains electroeluted from bands 1-3 containing the AgNP-chains has been presented in Figure 3.1(a). The absorption spectra of conjugated AgNP dimers and trimers are broader compared to the one obtained from single AgNPs (Fig. 3.1(c)), indicating plasmonic coupling between the particles.

20 nm *AuNP chains*

Linear chains of 20 nm AuNP conjugates containing discrete number of particles coated with G4-DNA were prepared as follows. 20 μL of G4-DNA solution in 10 mM of Na-Pi (pH 8.0) was prepared as described in 3.1.3 and mixed with freshly prepared AuNPs (OD 100), prepared as described in section 3.1.2. Then 4.3 μM Tris-Ac was added to the solution. Tris has been shown to induce the formation of chains of particles coated with G4-DNA [82]. The incubation was at 5 to 2 DNA to NP volume ratio for 5 minutes. Then the chain formation was halted by the addition of 20 μM $A_{10}a_5^*$ oligonucleotide. The oligonucleotide, in

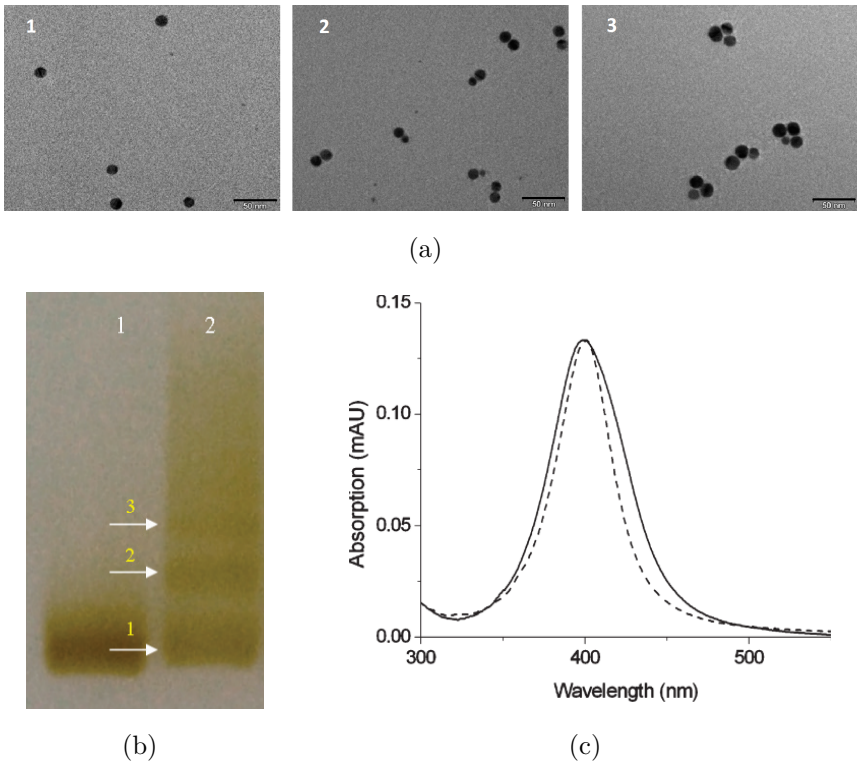

Figure 3.1. *Preparing of G4-AgNP-chain conjugates. (**a**) Chains of AgNPs containing a discrete number of particles electroeluted from an agarose gel (**b**) are prepared as described in [81]. (**c**) The absorption spectrum of an AgNP dimer is broader compared to single particles, indicating plasmonic coupling between the particles in the conjugate.*

addition to terminating chain growth, stabilizes the structures enabling their further separation by gel electrophoresis.

20 nm *AuNP flowers coated with G4-DNA*

AuNP "flowers" can be prepared by incubation of citrate-stabilized AuNPs (see 3.1.2) with 30-fold excess of AuNPs coated with 10 tetrad G4-DNA, as described in [83]. This procedure yields flower-shaped structures in which single uncoated AuNP is surrounded by 5-7 G4-DNA-coated particles within a planar arrangement shown in Figure 3.2(a). The particles are plasmonically coupled and the strength of the coupling depends on the length of the DNA-strands used for conjugation as evident from Figure 3.2(b).

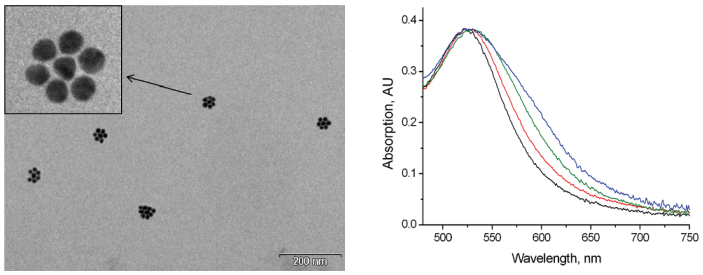

(a) (b)

Figure 3.2. *Preparation of* 20 nm *AuNP flowers conjugated with G4-DNA. (***a***) TEM images of prepared conjugates with scale bar of* 200 nm*. Flowers are prepared by conjugating citrate-capped* 20 nm *AuNPs with 10-tetrad G4-DNA coated ones. Central particles are surrounded by 5-7 particles. (***b***) Plasmonic coupling between the particles is affected by the length of the G4-strands. Black curve corresponds to absorption spectrum of* 20 nm *citrate-capped AuNPs, while red, green and blue curves correspond to 20, 10 and 5 tetrad-based NP-flowers. [83]*

60 nm *AuNPs coated with G4-DNA*

AuNPs with diameter of ≈ 60 nm were coated with both 10 and 30 tetrad G4-DNA functionalized with phosphorotioated adenosines. AuNPs (OD 20, see 3.1.2) were incubated in the presence of 20 µM G4-DNA in 10 mM Na-Pi for 45 minutes. LiCl was added to the concentration of 25 mM and the mixture was incubated for over-night. Then, LiCl concentration was increased to 50 mM and the incubation was continued for another 2 hours. Excess DNA was separated from the AuNP-G4 conjugates on a pre-packed Sephadex *CL-6B* column equilibrated with 10 mM Na-Pi (pH 8). Purple band was collected and the solution was centrifuged with Lumitron *eppendorf* centrifuge 5418 using 3,000 rpm for 6 minutes. The purity of the conjugates was further verified by gel electrophoresis in 1.25 % agarose gel.

3.1.5 Electrophoresis separation of particles in agarose gel

Gel electrophoresis is used to separate and purify samples by size and/or charge using an electric field. The migration speed of the macromolecules through the gel is inversely proportional to the size of the molecules, which allows size-dependent separation of the sample. The electrophoresis is typically used for separation and purification of DNA fragments. The technique can also be used to separate charged nanoparticles and conjugates, as was shown here.

Agarose gel was prepared using TAE x1 (Tris/Acetate/EDTA) buffer as the

medium. Agarose was added to the final concentration of 1.25-2 % depending on the size of the particles/conjugates being separated after which the mixture was heated in a microwave oven until the powder was completely melted. The gel was cooled down to 60 °C and then poured into a mould containing a sample comb. Once the gel was solidified the apparatus with the gel was filled with TAE buffer and the samples were loaded into the wells. Electric field was applied via a power supply. The voltage of 130 V was used and the runtime varied from about 30 minutes to 1 hour.

3.2 Dielectrophoresis

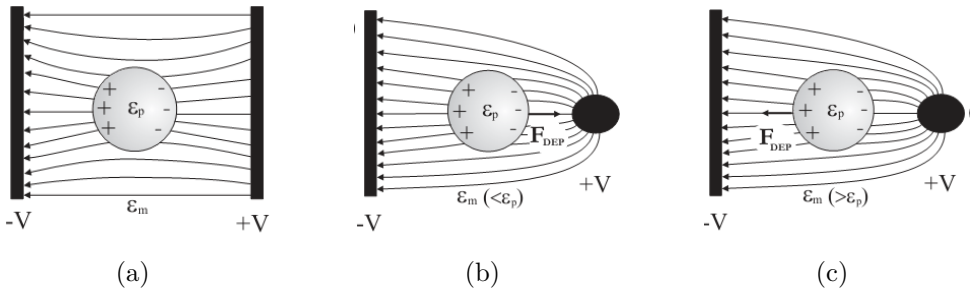

(a) (b) (c)

Figure 3.3. *The principle of dielectrophoresis phenomenon. (**a**) In an uniform electric field no net force is acting on a neutral polarizable object, whereas in a non-uniform electric field a net force is felt by the object. (**b**)* In positive DEP, the force is acting towards the field maximum and in negative DEP (**c**) towards the field minimum. Images are taken from reference [84].

When a dielectric (polarizable) object is subjected to a non-uniform electric field, a net force is exerted on the particle. This phenomenon is called dielectrophoresis (DEP). On contrary to the electrophoresis phenomenon, in which a charged object is moved by an electric field, in DEP the particle may be either charged or neutral. The principle of DEP is presented in Figure 3.3

In general, an external electric field induces opposite surface charges on each side of the polarizable object. These charges are of the same magnitude. If the external field is homogeneous, as in Fig. 3.3(a), no net force is acting on the particle due to Coulomb interactions acting with the same magnitude on the opposite sides of the particle. However, in a non-uniform electric field net force is generated as shown in Figures 3.3(b) and 3.3(c). For an ellipsoidal object time-averaged dielectrophoretic force is [85]

$$F_{\mathrm{DEP}} = \frac{\pi r^2 l}{3} \epsilon_m \cdot \mathrm{Re}(K(\omega)) \vec{\nabla} |\vec{E}|^2, \tag{3.3}$$

where ϵ_m is the electrical permittivity of the medium, r is the radius of the object, l the length, $K = \frac{\epsilon_p^* - \epsilon_m^*}{\epsilon_m^*}$ is the so called Clausius-Mossotti factor and E is the magnitude of the external electric field. Clausius-Mossotti factor depends on the complex permittivities of both the particle ϵ_p^* the medium ϵ_m^*, which are in turn dependent on the frequency of the external electric field ω. Furthermore, K determines whether the DEP force is positive or negative. When $\mathrm{Re}(K) > 0$, or $\epsilon_p^* > \epsilon_m^*$, DEP is positive and the force acts towards the field maximum, whereas when $\mathrm{Re}(K) < 0$ the force acts towards the field minimum (Fig.3.3(b) & 3.3(c)). In practice, field maxima are located at the corners and edges of the electrodes used for creating the electric field. From equation 3.3 it can be seen that the direction of the electric field does not affect the direction of the DEP force as the force is generated only by the field gradient. Thus, also AC fields, in addition to DC fields, can be used for DEP manipulation. Time-varying electric field cancels out the pure electrophoretic effect, which is advantageous in many cases.

Dielectrophoresis is a powerful tool for micro- and nanomanipulation due to its polarizability and thus size sensitivity. It has been utilized in wide range of environmental, biological and pharmaceutical applications for trapping and assembling, separation and sorting, patterning, purification and characterizing [86, 87, 88]. In our work DEP was utilized for trapping and immobilizing nanoparticles as a part of an electronic circuit.

In order to successfully manipulate particles using DEP, one needs to carefully consider the parameters. As can be seen from the equation 3.3, the DEP force is proportional to the volume of the particle. On the other hand, magnitude of Brownian motion is inversely proportional to the cube root of the volume [89], $F_\mathrm{b} \propto V^{-1/3}$, thus in order to manipulate relatively small particles high electric field gradients has to be used to overcome the effect of random movements. This sets the lower limit for the size of the particle. However, the definition of the nanoparticle size may not be always fully clear, since charged objects can contain counter-ion cloud around them, which can have significant affect on DEP.

The higher field gradients for successful trapping of nanoparticles can be generated by either reducing the dimensions of the electrodes or applying higher voltages to the electrodes. A conventional set up used for DEP trapping consists of two thin metal electrodes with a narrow gap between them. The scales can not be reduced limitlessly so for some applications higher voltages have to be used. However, practical reasons set limits for the applied voltage as there exists

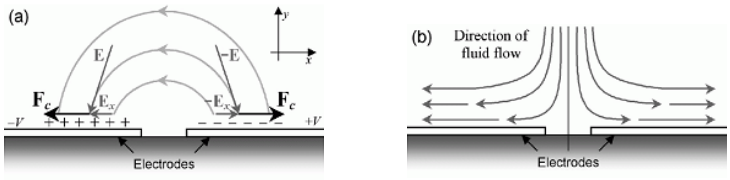

(a) (b)

Figure 3.4. *A schematic diagram of AC electro-osmosis for two nanoelectrodes separated by a narrow gap. A potential difference applied to the electrodes induces a charge layer and the electric field E, which has a tangential component E_x on the surface of the electrodes, presented in (***a***). This component produces a force F_c moving the induced charge layers away from the gap area. The resulting steady fluid flow dragging fluid down in the center of the gap and across the surface away from the gap area is presented in (***b***). [90]*

some undesired side-effects when using high voltages. Firstly, electric current going through the aquatic solution induces temperature gradients in the system. This phenomena is called Joule heating. Temperature changes in turn induce convection flows which may prevent trapping by moving the particles away from the gap area. Secondly, fluid flows may also be generated by AC electro-osmosis which is originated from the formation of an electrical double layer (EDL) at the interface between the electrode and the buffer solution.

According to Stern model [91] EDL is formed when ions are absorbed near a charged surface from the solution creating a net charge around the surface. This layer of ions is so-called compact layer. In turn, counter-ions are free to accumulate around the compact layer creating a so-called diffuse layer. The potential across EDL drops exponentially. External electric field induces movement of the ion layers through Coulomb interaction, thus creating fluid flows. In the case of two nanoelectrodes the Coulomb force is directed away from the gap area even if the electric field is time-varying (Fig. 3.4). Therefore higher electric field induces stronger fluid flows away from the gap which is very troublesome for the yield of the trapping.

3.3 Electrical measurements

In order to measure the conductance of the particles the conjugated structure under study was first trapped between two nanoelectrodes using dielectrophoresis. The same electrodes were also used for measuring the conductance of the trapped conjugate.

3.3.1 Fabrication of the fingertip-electrodes

Preparations

The nano-electrodes were fabricated using conventional electron-beam-lithography. The process begun by cutting a slightly *p*-doped silicon chip onto which the designed pattern was manufactured. The upper 100 nm layer of the silicon wafer was oxidized to form a layer of SiO_2. Silica is very stable in different conditions and, more importantly, electrically insulating. The chip was cleaned with hot acetone and subsequently with isopropanol. One minute sonication was used to take off any of the loose particles from the surface.

Thin film of resist was deposited while rapidly spinning the chip. Spinning ensured that the resist is thin and uniform enough. Resist in this case was 2% 950 PMMA A produced by MicroChem which is a positive resist, meaning that only the exposed areas are removed in developing. Spinning speed of 2000 rpm was used which lead to resist thickness of around 100 nm according to the manufacturer. After spincoating the chip was baked on a hot plate at 160 °C for 5 minutes.

Exposure

For the exposure *Raith e-Line* e-beam writer was used. As the electrodes for trapping should be as narrow as possible, the electron beam had to be focused on the surface of the resist with a great accuracy. Focusing could be done without using any contamination particles because *e-Line* software has a function which halts the beam in the centre of the screen during the imaging mode. If this is done while imaging the resist the electron beam burns the resist and collects unavoidable contamination particles from the vacuum chamber. The size and the shape of this contamination spot reveals whether the electron beam needs to be adjusted. For exposure under 20 nm contamination spot was required. The whole pattern was exposed using three different working fields and two different aperture sizes. Working field determines the used magnification and thus the area the beam can expose without moving the sample holder. By changing the aperture size the current going onto the sample can be modified. For the tips of the electrodes the smallest 10 µm working field with 10 µm aperture size was used to provide accurate enough results. This yielded a current of ≈ 0.040 µA. For middle regions connecting the narrow tips to the wide electrodes and contact pads working field was increased to 200 µm. The biggest structures were exposed with the biggest aperture size of 120 µm, yield-

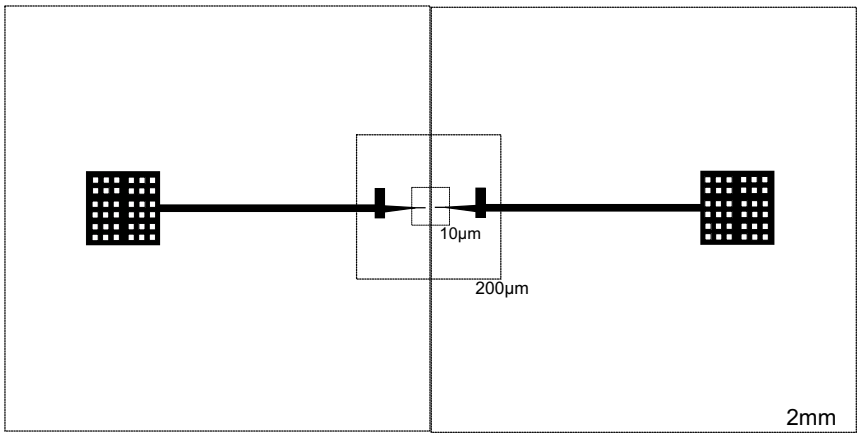

Figure 3.5. *Design of the fabricated structure. Three different working fields were used and presented in the figure. The outcome of the whole procedure is two fingertip-like electrodes having a width of* 20 nm *facing each other. The electrodes are connected to* $0.5 \times 0.5\,\mathrm{mm}^2$ *contact pads.*

ing a current of $\approx 5\,\mu$A, and by stitching two 2 mm working fields together. A clarifying presentation of working fields is presented in Figure 3.5.

Development

After exposure the sample was immersed for 30 s into a development solution containing methyl isobutyl ketone (MIBK) diluted to isopropanol with the ratio of 1:3. This solution dissolved only the exposed areas from the resist layer with very high resolution. The development was stopped with pure isopropanol. After development the chip was treated with a 10 s 15 W oxygen flash in a reactive ion etcher (RIE) in order to clear any PMMA residues from the developed areas which could affect the conductivity of the electrodes.

Metallization and lift-off

Metallization was done by coating the whole sample with a 2 nm layer of titanium and 20 nm or 50 nm layer of gold via e-beam evaporator in an ultra high vacuum (UHV) chamber. The thickness of the gold layer was matched with the size of the particle conjugates to be trapped. Titanium has a high adhesion to the surface and provides rougher surface, thus improving the contact for gold compared to a bare SiO_2 surface. This way the layer of gold stuck to the surface better and did not peel off from the surface during the lift-off process. Lift-off was done by leaving the sample in acetone for overnight. The chip containing one electrode-pair was gently rinsed with acetone after which short

sonification was used to remove the rest of the unwanted metal. Just before the dielectrophoretic trapping procedure the chip was treated with a 1 min 100 W oxygen flash in RIE in order to remove any residues left from the lift-off and to make the top of the hydrophobic silicon chip hydrophilic. An AFM image of a pair of nano-electrodes ready for the trapping procedure is presented in Figure 3.6.

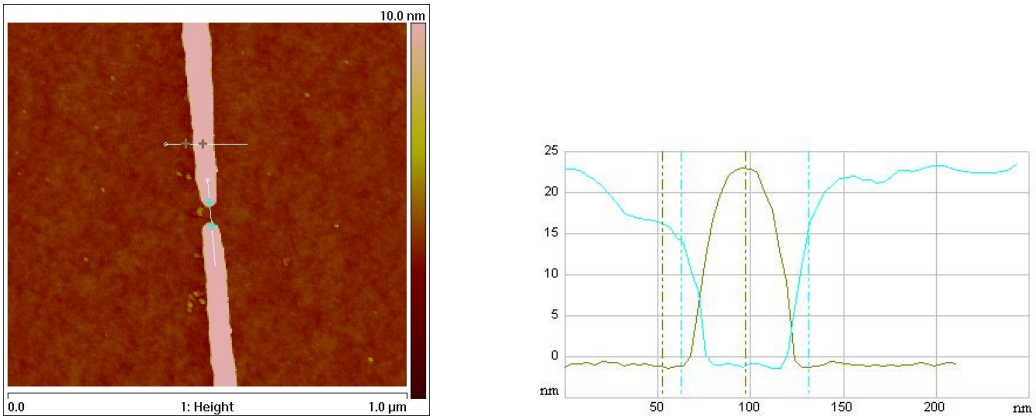

(a) Nano-electrodes (b) Section

Figure 3.6. *(**a**) An AFM image of a nano-electrode sample before the DEP-trapping procedure. Sample was fabricated by using the conventional electron-beam-lithography. As can be seen from the figure (**b**) the gap between these particular electrodes is about* 60 nm.

3.3.2 Dielectrophoretic trapping

The conjugated nanoparticle structures were positioned between the two gold-nanoelectrodes using the dielectrophoretic trapping procedure described in 3.2. The conjugate solutions were diluted with double-distilled water in order to reduce the concentration of the buffer present in the sample. Too high conductivity of the buffer induced unwanted electrothermic and AC electro-osmotic flows around the gap area as discussed in 3.2. In the worst case high current flowing through the narrow gold-electrodes destroyed the sample by melting. In order to prevent this, an additional 100 MΩ resistor was connected in series to reduce the current after successful trapping.

DEP trapping procedure was done inside enclosed sealed metallic box. The chip was placed on a nylon stage covered with epoxy. The sharp metallic probes of the stage were placed carefully on the pads of the sample. Probes were connected to a signal generator (Agilent 33120A waveform generator). Frequency

of the signal was varied between 1 kHz-15 MHz and the voltage in between 2.0-6.0 V.

A 5 µL drop of the sample was dropped on the centre of the electrodes. Water was poured into the box in order to increase the surrounding humidity an thus to prevent drying of the sample. During the DEP the box was closed and the AC voltage was set. Trapping time was varied from about 5 to 12 minutes depending on the concentration of the particles. After trapping was completed the chip was rinsed with double-distilled water and quickly dried by a nitrogen gas flow. The voltage was turned off, the chip was removed from the stage and treated for 10 seconds with a nitrogen flow to completely dry the chip. The presence of the nanoparticle structures between the electrodes was proven by using Veeco Dimension 3100 AFM. The DC conductivity measurements were done right after the imaging.

3.3.3 DC-conductance measurements

Conductance measurements were done by using the same nylon chip stage as used for the trapping procedure. Stage was placed inside an electrically sealed metallic box and the box was grounded to a specially built grounding point. All the measurements were conducted in an electromagnetically shielded room at an ambient temperature (21 °C). Humidity in the measurement box was measured by a HIH-3602-A Honeywell Humidity sensor.

Voltage between the electrodes was applied by using a battery-powered DAC circuit which was controlled by a specially programmed Labview-program. High voltages and quick voltage changes were avoided in order to prevent disintegration of the sample and accumulation of dirt. The current and voltage were measured using battery-powered preamplifiers (DL-Instruments Model 1211 and Model 1201, respectively). In the first measurements voltage was varied by finite steps of ≈ 5 mV in the range of ± 0.5 V. The range was gradually increased usually to ± 1.2 V. The positive and negative voltages were swept either separately or within the same cycle. The current and voltage signals were transferred to a computer through a data acquisition card (DAQ, National Instruments PXI-10311). One current-reading was acquired by averaging 1,000 individual readings and after each change of voltage the system was given at least 300 ms to settle. The internal scanning rate was 10,000 scans/s.

All the samples were measured in ambient conditions. Additionally measurements in high relative humidity (up to 90 %) were done for selected samples. The humidity in the sample box was slowly increased by flowing steam from

heated distilled water into the box while constantly sweeping the DC voltage and measuring the current.

4 Analysis and results

4.1 DEP trapping

The conjugates were immobilized between nanoelectrodes using DEP trapping procedure as described in 3.2. The yield of the trapping strongly depends on the voltage and frequency of the used AC signal. Using optimal parameters one can place a single conjugate between the electrodes. DEP parameters have been tested in NSC on various previous studies [92, 93]. These studies have demonstrated that using too low frequencies the conjugates are mainly lying on the electrodes and not in the gap between them, whereas at relatively high frequencies the conjugates tend to repel the electrodes due to the effects such as electro-osmotic and electrothermal flows. Also voltage has an affect to the intensity of the unwanted flows and in some cases the yield of the trapping is greater using relatively low voltages.

All these effects were evident also in this study. Also many electrodes were destroyed by melting during the trapping procedure. There was no clear correlation between the DEP parameters and the yield of the melting, i.e. using high DEP voltage did not necessarily yield melting of the electrodes. One explanation for this is that the successful trapping results in a sudden peak in the current over the capacitive coupling between the electrodes. To reduce this a resistor of up to $100\,\mathrm{M\Omega}$ was connected in series to the trapping set up. However, this did not reduce the yield of the melting dramatically. On the other hand, electrodes are capacitively coupled also with the ground through an electrically insulating layer of SiO_2 especially via contact pads. The sudden current destroying the electrodes may be originated from a charge stored in this capacitive coupling. Therefore increasing the resistance of the electrodes itself may increase the yield of the trapping. A few experiments using these kind of electrodes have been performed indicating very promising results. In this study two samples (Samples 11 & 12) were trapped using resistive electrodes with the resistance of $\sim 50\,\mathrm{k\Omega}$.

In this study we were able to position into the interelectrode gap a small

number (one to three) of conjugates of G4-AgNP-trimers, AuNP-flowers and G4-coated 40-60 nm AuNPs. The trapping was not successful for G4-coated AuNP chains consisting of 3-7 particles perhaps due to the low concentration of the samples and the conductivity of the buffer (1xTAE). The buffer could have been tried to be changed but the needed spin-filtering might have resulted the disintegration of the conjugates. Therefore, we decided to concentrate on the other samples.

4.2 Silver-nanoparticle conjugates

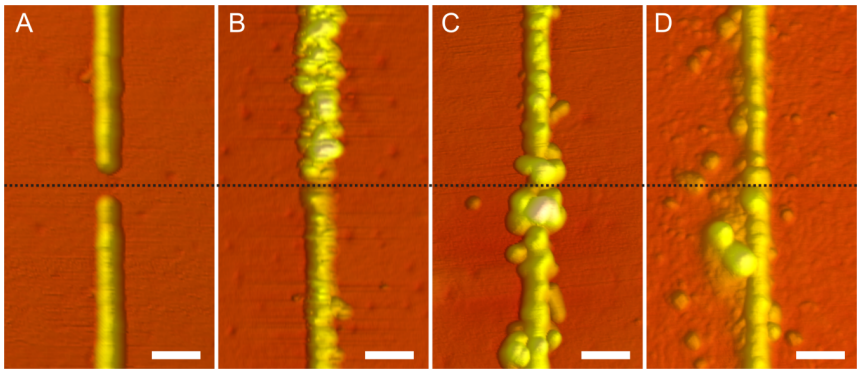

Figure 4.1. *AFM-images of empty lithographically fabricated gold nanoelectrodes (**a**) and electrodes with trapped G4-DNA-AgNP trimers (**b-d**). In **b** the trapping has not been successful, whereas **c** and **d** present successful result. Scale bars are* 100 nm *and the dotted line visualizes the position of the gap in each image. [94]*

G4-AgNP conjugates were prepared by the research group of Alexander Kotlyar (Tel Aviv University). Samples were shipped to NSC in order to perform electrical measurements on them. Samples were not exposed to any light during the shipping but the temperature may have varied, which in turn may have had an effect on the structure of the conjugates. However, AFM images confirmed that the samples indeed consisted of similar conjugates as presented in Fig. 3.1(a). As soon as the samples arrived, they were stored in a refrigerator (4 °C).

As presented in Figure 4.1 DEP trapping was successful on G4-DNA-AgNP trimers. In sample B DEP voltage was 3.5 V_{pp} (peak-to-peak voltage) and corresponding frequency 1 MHz. The same parameters were also used in sample C but the result is more successful as the conjugates have gathered closer to the interelectrode gap bridging it clearly by one or two conjugates. The difference in the results may be due to different properties of the buffer as the samples

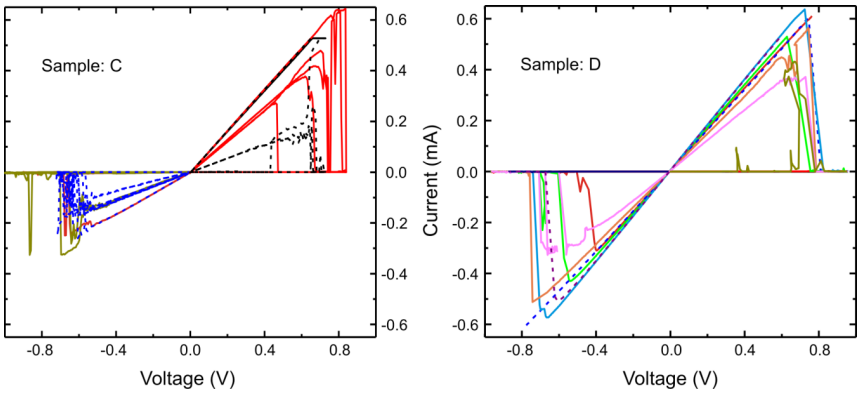

Figure 4.2. *I-V characteristics of Samples C and D (Fig. 4.1) measured in ambient conditions. Two conductive states are present (see text): high conductive states correspond to resistances of the order of* 1 kΩ *whereas the resistance of the non-conductive state is* ∼ 1 TΩ*. Reversible sharp switching between these states happens with potentials* ∼ ±0.7 V*. [94]*

were diluted with different ratios by water. Sample D was trapped using DEP voltage of 5.0 V and frequency of 5.0 MHz.

It has to be noted that the resistance of bare electrodes was shown to be more than 25 TΩ. Any decrease in the resistance is therefore attribute to the nanoparticle structures trapped bridging the interelectrode gap. The I-V curves of samples C and D (Fig. 4.2) are characterized by two clearly separate conductive states. Linear behaviour with low resistance (in the order of 1 kΩ) is evident in a range of ∼−0.7 V to +0.7 V. Increasing the absolute voltage outside this range result in a sharp increase of the resistance and decrease of the current. The resistance of the non-conductive state is of the order of 1 TΩ. The transition between the states is reversible and applying absolute voltage up to 1.2 V did not result in any irreversible changes in the DNA-NP system since the conductivity could always be restored by reducing the applied voltage. However, it has to be noted that the switching from low to high conductivity did not happen at every cycle. In some cases reducing the voltage below 0.7 V was not associated with an increase of the current. The I-V pattern, however, was always restored after one or several cycles. This was also supported by the fact that transition to the low conductivity state never happened if the voltage range did not exceed 0.7 V during the sweeping. On the other hand, after switching to the high conductivity state, it was never switched off while sweeping only within voltages of absolute value below 0.7 V. This unusual I-V behaviour was repeated totally on 5 different samples .

As can be seen from Figure 4.2, the resistance of the high conductivity state

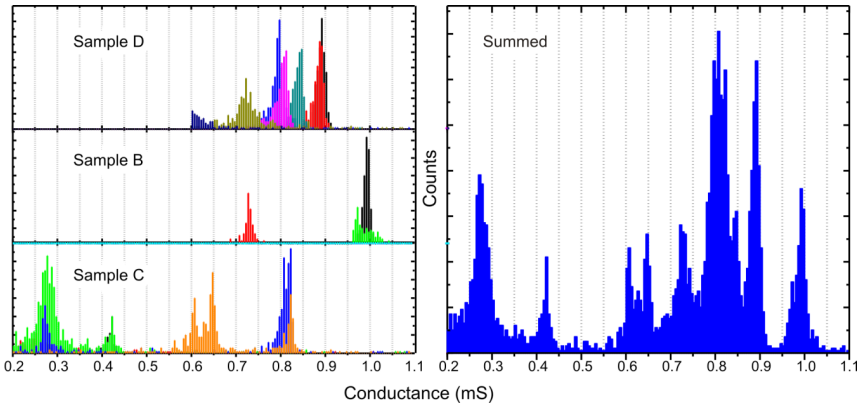

Figure 4.3. *The statistical analysis of conductance data collected from samples B, C and D. Derivative analyses of all I-V curves allowed estimation of possible discrete conductance values for samples D, B and C (left panels). Right panel summarizes statistical data obtained on the three above samples. [94]*

is varying from cycle to cycle in a random fashion. However, within same cycle the resistance is always constant. Switching to a non-conductive mode and getting back to a conductive one slightly changes the conductive characteristics. Statistical analysis of the low-resistance state conductance is presented in Figure 4.3. Interestingly there seems to be certain discrete peaks of the conductance which are shared between two different samples (0.82 mS in samples C and D and 0.72 mS in samples B and D). Summing data from samples B-D together reveals peaks separated by ~ 0.05 mS.

It could be speculated that the discrete conductive states correspond to electron transfer through particular G4-DNA molecules which orientation and nature can vary from cycle to cycle. It can be also suggested that the average difference corresponding to different peaks corresponds to the conductivity of a single G4-DNA molecule connecting the particles since the number of the strands is not precisely fixed either.

In order to distinguish the conductive characteristics of the G4-strands, measurements with Ag-NPs coated with poly-A oligonucleotides without G4-DNA linkers were also carried out. Results obtained from one of the samples are presented in Figure 4.4. Also this sample showed signs of ohmic linear resistance with same kind of switching properties. The resistance is at lowest of the order of 1 kΩ but the linear behaviour was more unpredictable and high conductivity state switched-off more easily than in the case of G4-DNA-AgNP trimers. The oligonucleotide layer makes assumingly direct contact between

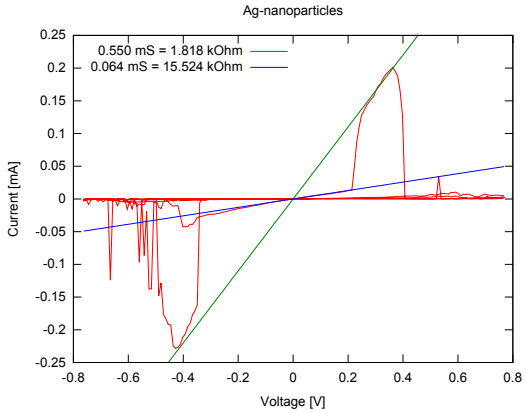

Figure 4.4. *DC I-V characteristics of a poly-A oligonucleotide coated AgNPs measured in ambient conditions. Both low (*$\sim 1\,\mathrm{k\Omega}$*) and high (*$\sim 1\,\mathrm{T\Omega}$*) resistance linear characteristics are present with sharp transitions between the conductivity states. The results are similar compared to the measurements made on G4-AgNP conjugates although the switching between states is much more unpredictable.*

the particles impossible. Therefore, layer of these short DNA-sequences have presumably some contribution to the electrical conductance of the synthesized structures also in the case of the G4-AgNP trimers.

Roughly corresponding results for both conjugated and non-conjugated AgNPs indicates that the high conductivity of switch-on state was not solely originated from the conductivity of G4-strands. However, using G4-strands to connect AgNPs we were able to fabricate a reversible molecular electronic switch with two distinguishable on/off states and rather precise on/off potential. A couple of similar molecular switches have been introduced but few have been realized experimentally. For example, a mechanically driven molecular switch with a conductance ratio of 10 to 1 was introduced rather recently by Tao *et al.* [95] who were able to control the conductance of a single pentaphenylene molecule by modulating the angle between a molecule and two metal electrodes.

To address the conductivity of G4-strands more carefully, we decided to fabricate other types of structures utilizing AuNPs. Measurements done on these conjugates are discussed in the next section.

4.3 Gold-nanoparticle conjugates

4.3.1 Linear 20 nm AuNP conjugates coated with G4-DNA

G4-DNA coated linear chains of AuNPs were prepared as described in section 3.1.4 by undersigned in Tel Aviv university. Both 10 and 30 tetrad G4-DNA were used for coating the particles. It was noticed that crucial step in the preparation of the conjugates was the incubation of the particles with Tris-Ac. The incubation time and the concentration of Tris-Ac determined the size of the agglomerates. The colour of the solution was observed as conjugated AuNPs developed purplish tint. About five minute incubation with the presence of 4.3 μM pH 7.4 Tris-Ac was sufficient for producing chains of particles consisting of 3-7 particles without notable aggregation. Incubation with the presence of phosporotiated G4-DNA stopped the reaction completely as the spectrum of the solution did not develop further.

Agarose gel run showed clear bands (Fig. 4.5(b)) corresponding to chains consisting of discrete number of particles verified by TEM analysis (Fig. 4.5(a)). Enhanced plasmonic coupling between the particles is clear and is verified by absorption measurements. Conjugates exhibit notable red-shift and the spectrum is broadened as shown in Figure 4.5(c). The shape of the spectrum is affected a little by the size (length) of the conjugates with longer conjugates having broader and more red-shifted spectrum, as was expected. However, the length of the G4-DNA strands did not have any affect to the optical properties. The stability of the conjugates was monitored and after one month no notable changes compared to the original spectra measured right after the agarose gel separation, were evident. The spectra were narrowed a little but red-shift and broadening compared to the spectrum of bare unconjugated particles was still clear. This demonstrates the stability of the conjugates. Bare citrate-stabilized nanoparticles tend to form aggregates but coating with the G4-DNA prevents such aggregation.

DEP trapping procedure was tried several times on linear G4-AuNP conjugates but none of the samples was successful. As speculated earlier, this was probably due to the low concentration of the sample and the conductivity of the buffer (1xTAE). High conductivity of the buffer creates unwanted electro-osmotic flows around the gap area during the DEP trapping procedure preventing the immobilization of the conjugates in the worst case. Also the concentration of the final product after agarose gel separation and electroelution was typically low.

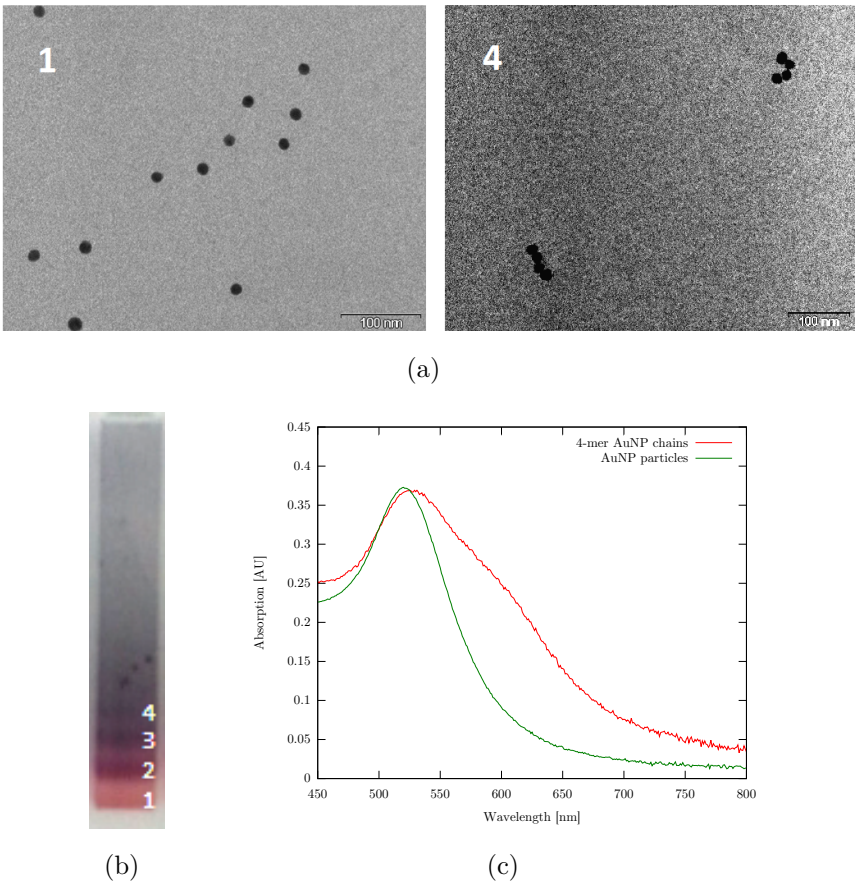

Figure 4.5. *Preparation of AuNP chains coated with G4-DNA. (**a**) TEM images of the conjugates separated from agarose gel separation bands (**b**). Bands were carefully cut with a razor blade and electroeluted into dialysis bags using 1xTAE buffer. The scale bars are* 100 nm. *Separated bands correspond to conjugates consisting of discrete number of particles. (**c**) Conjugates consisting of more than a single particle are characterized by a broadened absorption spectrum with considerable red-shift due to plasmonic coupling of the particles.*

4.3.2 G4-DNA-AuNP flower conjugates

G4-DNA-AuNP flower conjugates were prepared by the research group of Alexander Kotlyar. The samples were shipped to NSC and measured electrically.

AuNP flower conjugates were immobilized successfully between nanoelectrodes as shown in Figure 4.6. Both samples were trapped in 10 mM NaPi buffer using DEP voltage of 3.5 V, frequency 2.0 MHz, 15 min time and 1 MΩ front resistor. In Sample 7 (Fig. 4.6(a)) one of the flowers is clearly connecting the electrodes. The gap area is also surrounded by other conjugates which are not establishing electrical connection between the electrodes. Sample 8 (Fig. 4.6(b)) is not as clearly successful as the conjugate trapped between the electrodes is

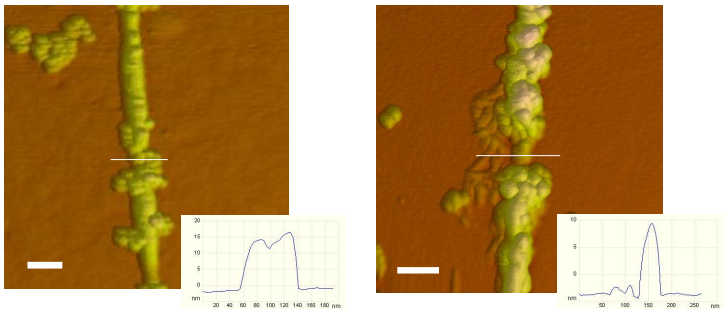

(a) Sample 7 (b) Sample 8

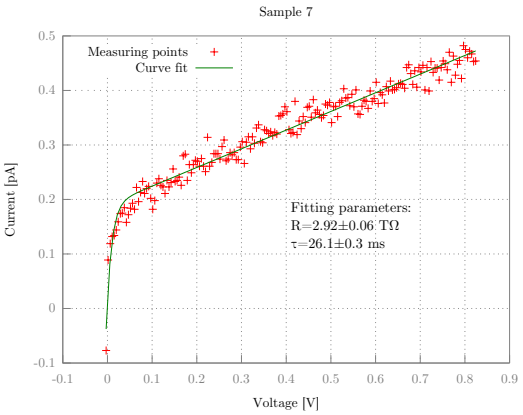

(c)

Figure 4.6. *AFM images of Sample 7 (**a**) and Sample 8 (**b**) with scale bars of* 200 nm *and typical I-V characteristics obtained in the dry environment from Sample 7 (**c**). The samples were G4-DNA AuNP "flower" conjugates. Resistance is of the order of* 3 TΩ*. Characteristics show hysteretic behaviour due to charging effects. Data has been fitted to the classical theory 4.1.*

rather obscure but it was measured electrically anyway.

Both samples (7 and 8) showed linear I-V characteristics with the resistance greater than 1 TΩ at small voltages and dry ambient environment. Resistance of the interelectrode connection is lowered by the conjugate compared to corresponding resistance of bare electrodes but the behaviour of G4-DNA is still insulating according to these results.

I-V characteristics exhibit hysteretic behaviour which can be explained by currents due to step-like charging of the total capacitance of the sample formed by the capacitance of the electrodes in addition to parasitic stray capacitances.

For step-like changing DC bias voltage one can derive [96] function

$$I = \frac{V_n}{R} + I_0 \alpha \frac{1-\alpha^n}{1-\alpha}, \tag{4.1}$$

where n is the nth point measured, V_n corresponding bias voltage, R the resistance of the sample and I_0 the maximum charging current at bias voltage transients (depends on the resistances of the measurement instruments). Parameter α describes the exponential ratio between the stabilization time τ_m (200 ms in our measurements) and the time constant of charging τ, $\alpha = \exp(\tau_m/\tau)$. Figure 4.6(c) shows a theoretical fit to the data obtained from Sample 7. From the fit resistance of 2.9 TΩ and time constant of 26 ms was obtained. Fitting a linear function to the linear part of the data points gives the resistance of 2.8 TΩ. The difference to the capacitive resistance is not significant and linear approximation is used in the analysis of the other similar results.

4.3.3 G4-DNA coated 60 nm AuNPs

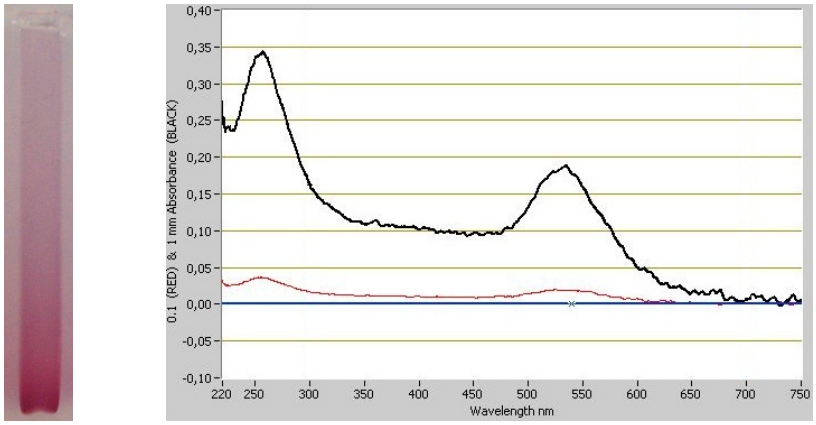

(a) (b)

Figure 4.7. *(**a**) Agarose gel electrophoresis run for 10 tetrad G4-DNA coated* 60 nm *AuNPs. The main band is clearly visible although little smear is present due to factors such as non-ideal concentration of agarose, excess of the sample or non-specific binding of DNA on the surface of AuNPs [45]. (**b**) Absorption characteristics of G4-DNA* 60 nm *AuNP conjugates with 20 tetrad G4 strands. The spectrum is recorded after spin-filtering the sample in order to remove excess non-conjugated DNA strands. As can be seen, the characteristic peaks of both DNA and AuNPs (at* 260 nm *and* 530 nm *respectively) are present. The black and red curves correspond to the* 1 mm *and* 0.1 mm *absorbance correspondingly.*

Incubation of 40-60 nm AuNPs with the presence of 10 and 30 tetrad G4-

DNA resulted in the formation of stable conjugates in the presence of up to 50 μM salt concentrations. 100 μM concentration of NaCl resulted in aggregation. The stability and uniformity of the conjugates was examined by agarose gel electrophoresis. The result is shown in Fig. 4.7(a). As can be seen, conjugates have entered the gel completely indicating that no notable amount of aggregates are formed. Also, only single band (with little smear) is visible indicating that only conjugates consisting of one single AuNP are present. The G4-DNA coverage of the AuNPs is therefore sufficient, meaning that G4-DNA strand, which has conjugated from the other end via sulphur link with a nanoparticle, has no room to conjugate to another particle. On the other hand, the present smear may indicate non-specific adsorption of G4-molecules on the surface of AuNPs, meaning that in addition to phosphorotioated adenines also other parts of DNA strands are bind with the gold atoms. This would cause variation on the effective diameter of the conjugates.

The benefit of higher ionic strength in the solution is the better DNA-strand coverage of the particles; the strands are driven closer to the particles for more efficient binding. However, it was demonstrated that practically all of the strands were conjugated with gold-particles. After 50 μM NaCl incubation of the G4-DNA and AuNP solution the mixture was spin-filtered with VWR PES, 30kD filter, which allows single G4-DNA strands to go through, whereas the conjugates do not pass through. The solution gone through the filter did not contain any trace of DNA indicating that the conjugation with the particles was successful. The spectrum obtained from the conjugates extracted from the filter revealed the characteristic peaks of both AuNPs and DNA, as shown in Fig. 4.7(b). Therefore, it can be concluded that both the DNA coverage of the particles is sufficient and the yield of the conjugation is high with the used salt concentration.

Figure 4.8 represent five successful DEP trappings of 40-60 nm AuNPs coated with 10 or 30 tetrad G4-DNA. The buffer in all the samples was 6.5 mM Hepes, 1 mM MgAc (pH 7) and 0.5 mM NaPi and the DEP frequency was 15 MHz. The voltage varied from 0.4 V_{pp} to 1.2 V_{pp}. Higher voltage was used for Samples 11 and 12 with resistive electrodes. The higher DEP frequency seemed to have higher yield in contrast to the 10 mM NaPi buffer used for trapping AuNP flowers for which relatively low frequency was used. In dry conditions the I-V characteristics of all samples exhibited linear behaviour with high resistance (1-5 TΩ) corresponding to the results obtained from the G4-AuNP flowers.

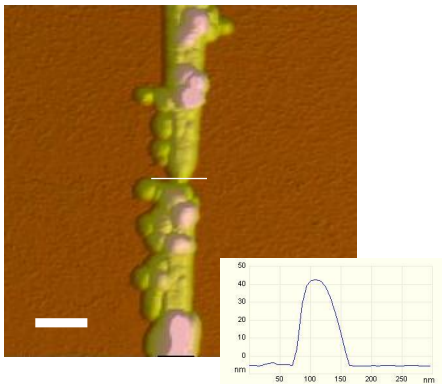

(a) Sample 148

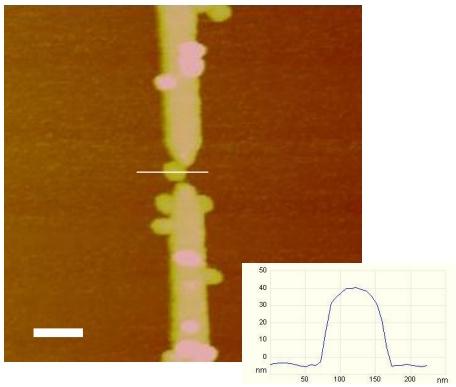

(b) Sample 149

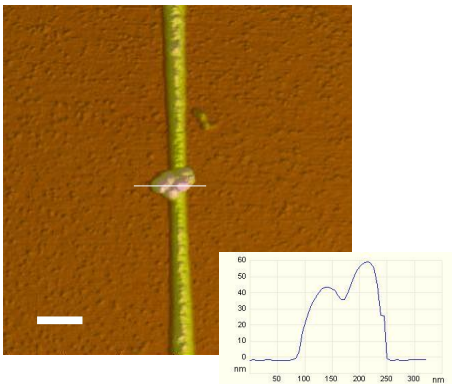

(c) Sample 11

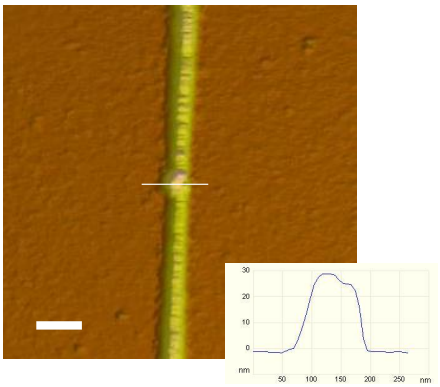

(d) Sample 12

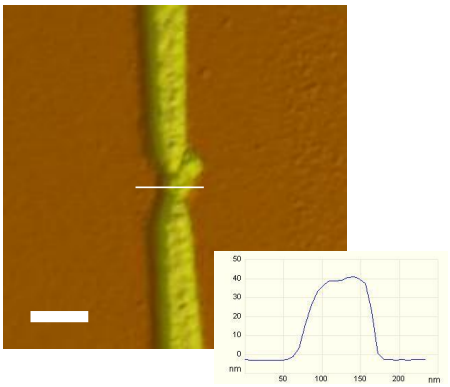

(e) Sample 128

Figure 4.8. *G4-DNA-AuNP conjugate samples after DEP trapping and before electrical measurements. (**a**) and (**b**): 40-60 nm AuNPs coated with 10 tetrad G and (**c**) to (**e**) 40-60 nm AuNPs coated with 30 tetrad G4. The scale bars in all the images are 100 nm.*

4.4 Discussion

Based on the AuNP-G4 measurements it can be speculated that the G4-DNA in the dry form does not adapt a configuration suitable for DC conductivity although the structure is very rigid [97]. In many studies the varying environmental conditions have been shown to alter the configuration of the dsDNA [98, 99] and this is most probably the case also with the G4-structure. Many studies confirm the insulating behaviour of DNA [100] in dry environment suggesting that DNA is significantly deformed from its natural state during the drying with a nitrogen flow.

Comparing the results of 60 nm AuNPs with the ones obtained from the G4-AuNP conjugates confirms the claim that the high electronic conductivity in the measurements on G4-AgNP conjugates was originated at least partially from the direct contact between the Ag-particles in the gap and the nanoelectrodes. In the case of the G4-AuNP conjugates direct contact between the particles is more unlikely as the particles are coated with considerable stiffer layer of DNA. Although the single-stranded polyA oligonucleotides covering the AgNPs may decrease the interactions between the nanoparticles in colloidal solution compared to the uncoated particles, in dry conditions ssDNA is expected to collapse more dramatically compared to the G4-structures in the AuNP conjugates making the direct metallic contacts more probable.

In the AgNP chains particles were conjugated by only a small number of G4-strands making the overall structure relatively flexible. Therefore, it is possible that the electric field generated by the bias voltage altered the configuration of the trapped conjugate making the direct metallic connection possible. In addition, the electric field may induce chemical changes of the G-basis at high redox potentials, thus perturbing the overall G4-structure. Thus, reversible switching between the conductive and insulating states is possible due to conformation changes in the G4-structures. However, none of the G4-AuNP conjugates showed such reversible switching behaviour indicating the change in the G4-strand configuration is more probably driven by mechanical stretching along the electrode axes in the electric field. In G4-AuNP conjugates more rigid layer of DNA did not allow such stretching. In conclusion, the switching potential of $\pm 0.7\,\mathrm{V}$ of the G4-AgNP chains may be linked to the stiffness of the G4-structures.

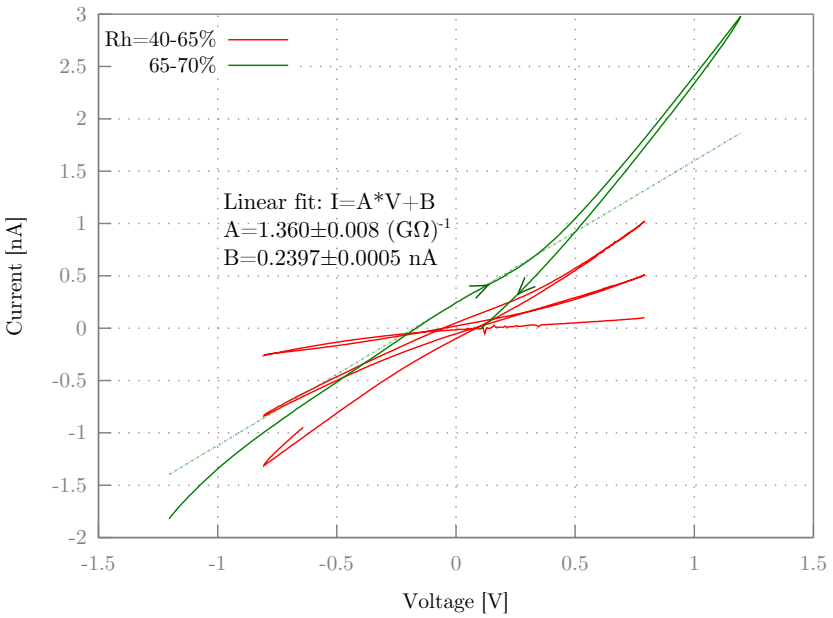

(a) Sample 11

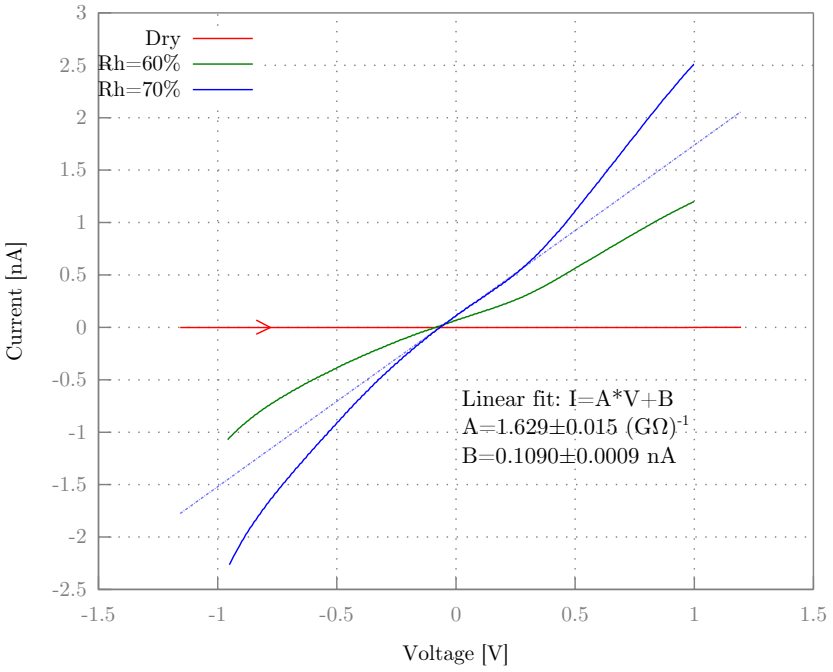

(b) Sample 12

Figure 4.9. *I-V characteristics of Samples 11 (**a**) and 12 (**b**) in increasing humidity. The direction of the change of the bias voltage is indicated by arrows. Resistances at* 0.1 V *were determined by fitting a line to the data points in the range of* 0.05 *to* 0.15 V.

4.5 Measurements at high humidity

In addition to dry conditions, measurements in high RH (up to 80%) were made on G4-coated 60 nm AuNPs. In all of the samples the resistance dropped to lower than 10 GΩ (down to $\sim$ 0.3 GΩ) whereas the resistance of bare electrodes in the same conditions was of the order of $\sim$ 0.2 TΩ. In high relative humidity all the samples exhibit non-linear I-V characteristics with typical S-shape, which has been reported earlier for other DNA derivatives [71] and G4-structure [76]. The resistance is rather constant in the range of ~ -0.3 to 0.3 V outside of which the resistance is decreased to roughly half.

Figure 4.9(a) shows DC I-V characteristics obtained from a 60 nm AuNP Sample 11 in varying relative humidity. The resistance in the dry environment was 2.7 TΩ. Conductance is increased rather exponentially as the function of relative humidity. In humidity of $\sim$ 70 % the resistance in the range of ~ -0.3 to 0.3 V is decreased to 0.74 GΩ. Above absolute potential of $\pm$0.3 V the resistance is 0.36 GΩ with linear I-V characteristics. Similar "kink" in the curves is evident also in the characteristics obtained from Sample 12 (Fig. 4.9(b)) and Sample 149 (Fig. 4.10(a)) roughly at the same potential. Sample 12 showed the resistance of 0.61 GΩ at low absolute potentials and 0.35 GΩ elsewhere. Corresponding resistances for Sample 149 were 11 GΩ and 3.6 GΩ. The higher resistance for the latter sample can be explained by poorer connections compared to the other samples as the AFM image shows a probable gap between the other electrode and the conjugate. Sample 148 (Fig. 4.10(b)) was measured only in the dry environment showing linear characteristics with varying resistances ($\sim$ 4.0-9.0 TΩ).

Similar increase in the conductance at certain threshold voltage ($\sim$ 0.5 V) in high humidity was evident also with bare electrodes without bridging conjugates (Fig. 5.1 in the Appendixes), although the effect was not as clear. In an earlier work [101] with DNA origami structures it was reported that this kind of change in conductance can be explained by some redox reactions on the Au-electrodes. It is also possible that such reactions happen also in the AuNPs even easier than on the electrodes. Alternatively some redox reactions may happen in the G4-structures. Kleine-Ostmann *et al.* [71] reported very similar S-shaped I-V characteristics for dsDNA on Au nanocontacts. They explained the behaviour by the dissociation of water attached to the DNA molecules as the effect was also evident for denatured DNA. However potential of $\sim$ 0.3 V is not high enough for this explanation to be relevant in our experiment [102]. It is also possible that the origin of the increased conductivity above the threshold

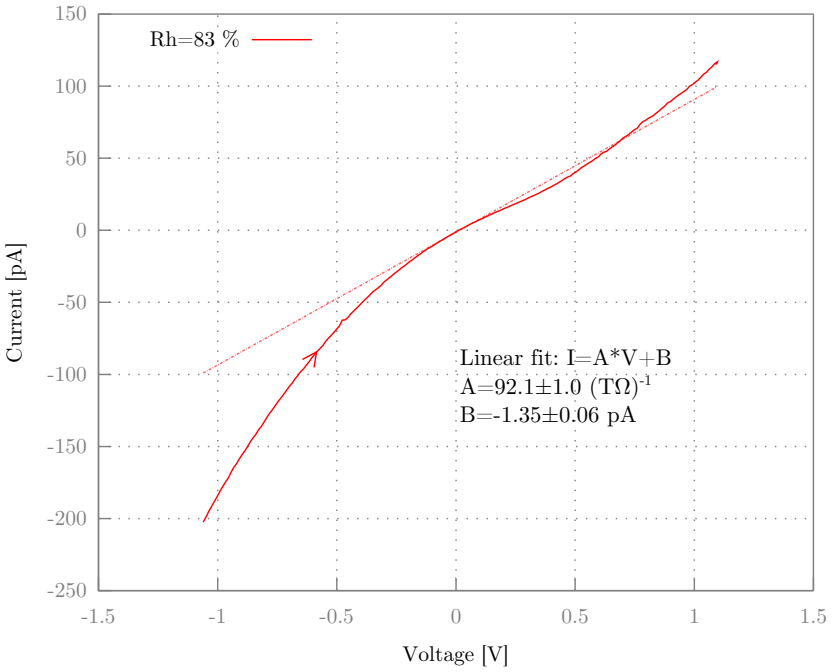

(a) Sample 149

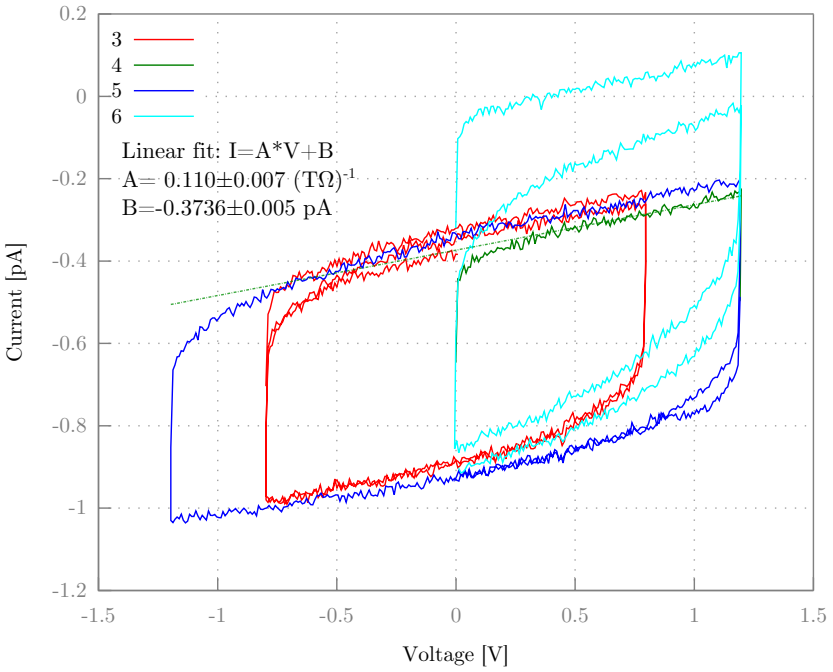

(b) Sample 148

Figure 4.10. *I-V characteristics of Samples 149 (**a**) and 148 (**b**). Curve for Sample 149 was measured in RH of 83 %, whereas Sample 148 was measured only in ambient conditions (RH ∼ 23 %). The direction of the change of the bias voltage is indicated by an arrow. Resistances at* 0.1 V *were determined by fitting a line to the data points in the range of* 0.05 *to* 0.15 V.

voltage of 0.3 V may be some electron/hole tunnelling processes, which become available at high RH.

The measured minimum resistance of $\sim 0.4\,\mathrm{G\Omega}$ in the relative humidity of 80 % corresponds roughly to the experimental results obtained by Liu *et al.* [76] who measured the resistance of G4-structures in the buffer. The reported resistances at bias voltage of 0.1 V varied in the range of 10^7-$10^9\,\Omega$. It has to be also noted that the structures were shorter (3 tetrad) compared to the ones used in our work (10-30 tetrad). However, the potential for the electrical conduction seems to be lost in the dry environment according to the our results obtained from the AuNP conjugates. This may be due to various reasons. As stated, the G4-structures may be considerably deformed due to absence of buffer or the interactions with the substrate surface altering the π-orbital overlap of the bases and suppressing the electron transport/transfer along the G4-strand. The suppressed conductivity may also be originated from the absence of counter-ions if the conductance is mainly ionic. In an earlier work [101] it was reported that the conductance of the DNA-origami structures have both electronic and ionic contribution which may be true also for the G4-structures. However, based on the experiments reported here the nature of the charge transfer of G4-DNA cannot be carefully determined.

The influence of the relative humidity on the resistance was examined more carefully with data obtained from Samples 11 and 12. Resistance at bias voltage of 0.1 V was obtained by fitting a line to the I-V curves in the range of 0.05 - 0.15 V. The resistances plotted as the function of RH and compared to the results obtained from an empty sample (bare electrodes which underwent the same trapping procedure expect without DNA) are presented in Figure 4.11. As can be seen, the resistance of the empty sample behaves purely exponentially as the function of humidity, whereas the resistance of Samples 11 and 12 are decaying faster at low humidity levels. At humidities higher than 40 - 50 % the decay of the resistance is settled to the same level as in the empty sample.

The dramatic difference between the empty sample and the samples with G4-AuNP conjugates indicates that the conductance properties of G4-structures can be altered by changing RH. Many studies have shown that RH has a major impact on the configuration of DNA [98, 99]. For example, natural B-DNA undergoes conformational change upon dehydration between RH 92 % and 70 %. Further decreasing of RH at room temperature reduces natural DNA to undergo denaturation [103]. The change of a conformation would have a significant affect on the π-stacking configuration of the DNA strand thus possibly

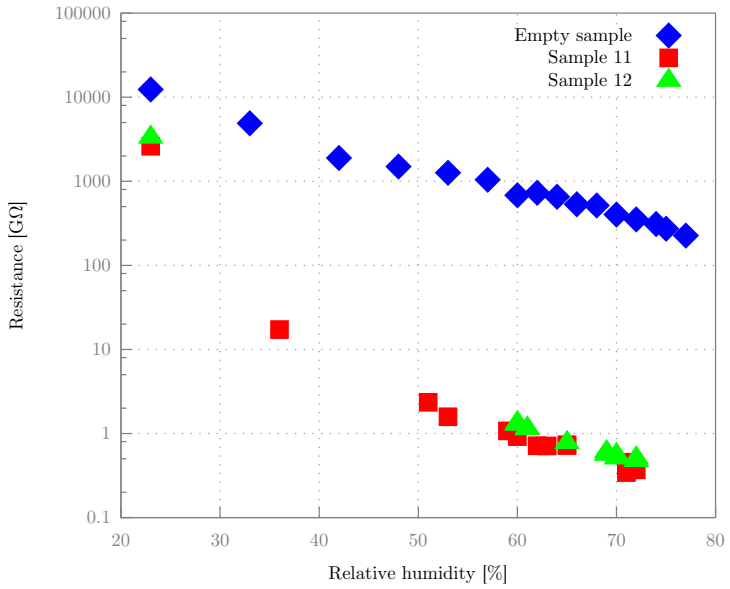

Figure 4.11. *Resistances of Samples 11, 12 and an empty sample (bare electrodes) at* 0.1 V *as the function of the relative humidity. Note the logarithmic scale on y-axis. The resistance of the bare electrodes decreases exponentially as the function of the humidity, as expected, due to increasing layer of water adsorbed on the* SiO_2 *surface. However, the behaviour of Samples 11 and 12 is not purely exponential as the decay of the resistance is varying as the function of humidity.*

altering the conductance properties. RH may have similar effect on the conformation of G4-structures and according to our results RH of 40 - 50 % may be so called critical RH which is needed to stabilize the G4-DNA. Above this RH the conformation would be fully native and the current carrying capacity at the maximum, thus increasing RH further would decrease the resistance only due to the increased conductivity of adsorbed layers of water.

Other explanation for the faster decay of the resistance in the humidities below 50 % with the conjugate samples would be that G4-DNA traps water molecules efficiently into its structure, thus creating highly arranged conductive channels. At $\sim$ 50 % all of the water molecule binding sites of G4 would be occupied and the conductance continues to increase only due to adsorbed layers of water. However, in earlier work with TX-tiles and origami structures [104, 105] the resistances followed a single exponential curve as the function of RH, which is not the case here. Therefore, ionic conductivity is not likely to explain all the contribution to the conductivity.

The conductivity of G4-DNA has been reported to be better compared to

dsDNA both by experimental [106] and theoretical [107] studies which is confirmed by also our work comparing these results to the ones obtained earlier for both individual dsDNA strands [49] and DNA origami structures [101]. These experiments were made utilizing exactly the same type of set-up. For origami structures in the relative humidity of 90 % the resistance of $\sim 10\,\mathrm{G\Omega}$ in the bias voltage range of -0.2 to $0.2\,\mathrm{V}$ and about $2\,\mathrm{G\Omega}$ outside this region was reported having therefore a tenfold difference to our results for G4-structures. However, it has to be noted that the hexanethiol linkers used to connect the origami to the nanoelectrode circuit are reported to have a resistance of $10\,\mathrm{M\Omega}$ - $1\,\mathrm{G\Omega}$. In similar conditions for a bundle of dsDNA molecules the resistance of 250-$700\,\mathrm{M\Omega}$ was reported which corresponds to the results reported here. However, in dry conditions dsDNA showed resistance of the order of $10\,\mathrm{T\Omega}$ compared to the lowest resistance of $1\,\mathrm{T\Omega}$ obtained from our work. Therefore, G4-DNA may sustain its conformation better compared to dsDNA or alternatively it binds more efficiently counter-ions, which may contribute to the electron transfer. On the other hand the distance travelled by electrons along DNA is longer in the case of origami structures compared to the conjugates measured in this work, which may explain the differences at least partly.

5 Conclusions

DNA has many useful characteristics, such as superior self assemblic properties, which make it a promising candidate for constructing nanoscale devices. Electrical conductivity of DNA has been under vigorous investigation for decades and there are still many unanswered questions related to the topic since the results have varied widely. However, it has been widely accepted that under ambient conditions natural double-stranded DNA exhibits insulating behaviour. The conductivity of DNA strands can be altered by changing the nucleotide composition with G-rich sequences having the best conductivity due to the lowest ionization potential amongst the nucleotides. Therefore, it has been proposed that G4-DNA may possess superior electrical conductivity compared to dsDNA. Also the structure of G4-DNA has been shown to be more rigid compared to dsDNA which would indicate that it is more stable under various environmental conditions. Preparing of different G4-DNA-metal-nanoparticle conjugates and determining the electrical conductivity properties of them was the main interest in the work described in this thesis.

The conjugates were measured electrically by DEP-trapping them between two gold-nanoelectrodes. Dielectrophoresis is a powerful tool for nanomanipulation as have been demonstrated here and in many other previous works. DC I-V characteristics were measured by applying bias voltage between the electrodes and measuring current going through the circuit. Both silver- and gold-nanoparticle conjugates were measured electrically. G4-AgNP conjugates were chain-like composing of 3 20 nm A-oligonucleotide coated particles connected with strands of 20 tetrad thiol-modified G4-DNA. They exhibited unusual "switching" behaviour with highly conductive state ($R \sim 1\,\mathrm{k\Omega}$) at voltages in the range of -0.7 to $0.7\,\mathrm{V}$. At voltages below $-0.7\,\mathrm{V}$ or above $0.7\,\mathrm{V}$ the conjugates behaved non-conductive with resistance of the order of $1\,\mathrm{T\Omega}$. The switch between the two distinct states was reversible and regular.

Two types of G4-AuNP conjugates were measured electrically in this work: flower-like planar arrangement of 20 nm AuNPs coated with G4-DNA and single G4-DNA coated 60 nm particles. Both types of conjugates exhibited high

resistivity ($R > 1\,\mathrm{T\Omega}$) in ambient conditions and no similar switching phenomena, as was the case with AgNP conjugates, was evident. On the other hand, bare AuNPs and A-oligo coated AgNPs exhibited low resistance ($R \sim 1\,\mathrm{k\Omega}$) linear I-V characteristics which would indicate that the high conductivity state of the AgNP chains was originated from direct contacts of the nanoparticles. Reversible switching can be associated to many sources of contributions. One can speculate that the reason for the unusual electrical behaviour demonstrated here can be associated also with detachment of the nanoparticles from the electrodes or from each other at high absolute values of voltage. As NP-DNA conjugates and metal particles can move towards cathode at relatively high values of the applied potential, movement along the electrode plane might physically detach the conjugates from the electrodes leading to transition of the system to the non-conductive state. However, it is most likely that changing of the conjugate position with respect to the electrodes would irreversibly abolish the conductance, which is not the case here.

Switching phenomenon can be also associated with changes of the G4 structure induced by the electrical field. Many studies have shown that the DNA conformation has a major impact on its electrical conductivity [65, 108]. The conformational changes can be driven by stretching the DNA during the conjugate movement along the electrode axes in the electrical field or by chemical changes of the G-basis at high redox potentials. It is well known that the G-base characterized by relatively low value of ionization potential, can undergo reversible redox transition at potentials higher than $+0.7\,\mathrm{V}$ or lower than $-0.7\,\mathrm{V}$ [109, 110]. The perturbation of the DNA structure induced by oxidation or reduction can lead to a sharp drop of the current at relatively low or high applied potentials. The π-stacking configuration of the DNA strand may be then altered to more unfavourable for charge transfer thus decreasing the conductivity. Alternatively, change of a DNA conformation may enable direct contact between the metal-nanoparticles, which is more likely explanation according to the results obtained in this work since AuNP conjugates did not exhibit high conductance I-V characteristics. The difference between Ag- and AuNP conjugates was the coating of the particles used for stabilization. Ag-particles were coated with single-stranded polyA-oligonucleotides whereas Au-particles were coated with more rigid G4-DNA. Therefore direct connection between AgNPs was more likely compared to AuNPs in the prepared conjugates. It can be speculated that the switch-on/off potential of $\pm 0.7\,\mathrm{V}$ with AgNP chains is linked to the stiffness of either G4-structures or A-oligonucleotides.

Measurements in increasing relative humidity (RH) were made on 60 nm G4-AuNPs and R-RH characteristics were obtained. Control samples (bare nanoelectrodes without bridging conjugate) show exponential behaviour over the range of 20 - 80 % RH due to water being the main charge carrier [111]. However, with G4-AuNPs the behaviour was different with the resistance decreasing more rapidly with low values of RH. At RH over 40 - 50 % the decay of resistance is settled to the similar level as in the control sample. Different R-RH characteristics of G4-AuNP and control samples indicate that the intrinsic conductivity of G4-DNA is increased by increasing RH. According to this result, the humidity of 40 - 50 % may be associated to the critical humidity of G4-structures, which would be needed to stabilize the structures.

Bibliography

[1] D. L. Nelson, Cox Lehninger, W.H. Freeman: *Lehninger's Principles of Biochemistry*, W H Freeman & Co (2004), ISBN 9780716771081

[2] E. Chargaff: *"Chemical specificity of nucleic acids and mechanism of their enzymatic degradation"*, Experientia 6 (1950), 201-209

[3] J. Watson and F. Crick: *"Molecular structure of nucleic acids"*, Resonance 9 (2004), 96-98

[4] Valentino R. Cooper *et al.*: *"Stacking Interactions and the Twist of DNA"*, J. Am. Chem. Soc. 130 (2008), 1304-1308

[5] C. R. Calladine: *"Understanding DNA: The Molecule & How It Works"*, Academic Press, 3rd ed., (2004)

[6] A. Ghosh, M. Bansal: *"A glossary of DNA structures from A to Z"*. Acta Crystallogr. 59 (2003), 620-626

[7] N. Maizels: *"Dynamic roles for G4 DNA in the biology of eukaryotic cells"*, Nature Structural & Molecular Biology 13 (2006), 620-626

[8] D. Sen & W. Gilbert: *"Formation of parallel four-stranded complexes by guanine rich motifs in DNA and its implications for meiosis"*, Nature 334 (1988), 364-366

[9] De Bizemont, J.-S. Sun, T. Garestier, and C. Helene: *"New junction models for alternate-strand triple-helix formation"*, Chemistry & Biology 5 (1998), 755-762

[10] M. Lu, Q. Guo, and N. R. Kallenbach: *"Thermodynamics of G-tetraplex formation by telomeric DNAs"*, Biochemistry 32 (1993), 598-601

[11] M. L. Bochman, K. Paeschke & V. A. Zakian: *"DNA secondary structures: Stability and function of G-quadruplex structures"*, Nature Reviews Genetics 13 (2012), 770-780

[12] T. Simonsson: *"G-quadruplex DNA structures variations on a theme"*, Biol. Chem. 382 (2001), 621-628

[13] S.M. Kerwin: *"G-Quadruplex DNA as a target for drug design"*, Curr. Pharm. Des. 6 (2000), 441-478

[14] W.I. Sundquist & Klug,A.: *"Telomeric DNA dimerizes by formation of guanine tetrads between hairpin loops"*, Nature 342 (1989), 825-829

[15] C. B. Reese: *"Oligo- and poly-nucleotides: 50 years of chemical synthesis"*, Org. Biomol. Chem. 3 (2005), 3851-3868

[16] W. P.C. Stemmer, A. Crameri, K. D. Ha, T. M. Brennan & H. L. Heyneker: *"Single-step assembly of a gene and entire plasmid from large numbers of oligodeoxyribonucleotides"*, Gene 164 (1995), 49-53

[17] S. Primrose, R. Old: *"Principles of gene manipulation: an introduction to genetic engineering"*, Oxford: Blackwell Scientific, (1994)

[18] S. Ha Park: *"Self-assembled DNA nanostructures and DNA-templated silver nanowires"*, Duke University, (2005)

[19] N. C. Seeman,: *"Nucleic acid junctions and lattice"*, Journal of Theoretical Biology 99 (1982), 2, 237-247

[20] J. Chen, N. C. Seeman, *"Synthesis from DNA of a molecule with the connectivity of a cube"*, Nature 350 (1991), 631

[21] P.W.K. Rothemund: *"Folding DNA to create nanoscale shapes and patterns"*, Nature 440 (2006), 297-302

[22] A. Rajendran, M. Endo & H. Sugiyama: *"DNA Origami: Synthesis and Self-Assembly"*, Current Protocols in Nucleic Acid Chemistry 12.9.1-12.9.18, John Wiley & Sons, Inc. (2012)

[23] S.M. Douglas, H. Dietz, T. Liedl, B. Högberg, F. Graf & W.M. Shih: *"Self-assembly of DNA into nanoscale three dimensional shapes"*, Nature 459 (2009), 414-418

[24] R. Jin et al.: *"Photoinduced Conversion of Silver Nanospheres to Nanoprisms"*, Science 294 (2001), 1901

[25] A. Roucoux, J. Schulz, H. Patin: *"Reduced Transition Metal Colloids: A Novel Family of Reusable Catalysts"*, Chemical Reviews 102 (2002), 3757-3778

[26] S. J. Park, A. A. Lazarides, C. A. Mirkin, P. W. Brazis, C. R. Kannewurf & R. L. Letsinger: *"The electrical properties of gold nanoparticle assemblies linked by DNA"*. Angew. Chem., Int. Ed. 39 (2000), 3845

[27] Jwa-Min Nam, C. Shad Thaxton, Chad A. Mirkin: *"Nanoparticle-Based Bio Bar Codes for the Ultrasensitive Detection of Proteins"*, Science 301 (2003), 1884-1886

[28] N. L. Rosi & C. A. Mirkin: *"Nanostructures in Biodiagnostics"*, Chem. Rev. 105 (2005), 1547-1562

[29] S. Eustis & M. A. El-Sayed: *"Why gold nanoparticles are more precious than pretty gold: Noble metal surface plasmon resonance and its enhancement of the radiative and nonradiative properties of nanocrystals of different shapes"*. Chem. Soc. Rev. 35 (2006), 209-217

[30] N. L. Rosi & C. A. Mirkin: *"Nanostructures in biodiagnostics"*, Chem. Rev. 105 (2005), 1547-1562

[31] Reichert technologies web site: `http://www.reichert.com/life_sciences.cfm`, accessed 20.3.2013

[32] S. K. Ghosh & T. Pa: *"Interparticle Coupling Effect on the Surface Plasmon Resonance of Gold Nanoparticles: From Theory to Applications"*, Chem. Rev. 107 (2007), 4797-4862

[33] Ian Chopra: *"The increasing use of silver-based products as antimicrobial agents: a useful development or a cause for concern?"*, Journal of Antimicrobial Chemotherapy 59 (2007), 587-590

[34] D. Manno, E. Filippo, M. Giulio & A. Serra: *"Synthesis and characterization of starch-stabilized Ag nanostructures for sensors applications"*, J. Non-Cryst Solids 354 (2008), 5515-5520

[35] J. Köhler, L. Abahmane, J. Albert & G. Mayer: *"Preparation of metal nanoparticles with varied composition for catalytical applications in microreactors"*, Chem. Eng. Sci. 63 (2008), 5048-5055

[36] J. Guo, H. Cui, W. Zhou, W. Wang: *"Ag nanoparticle-catalyzed chemiluminescent reaction between luminol and hydrogen peroxide"*, J. Photochem. Photobiol. A 193 (2008), 89-96

[37] Y.C. Hung, W.T. Hsu, T.Y. Lin & L. Fruk: *"Photoinduced write-once read-many-times memory device based on DNA biopolymer nanocomposite"*, Appl. Phys. Lett. 99 (2011), 253-301

[38] M.A. El-Sayed: *"Some Interesting Properties of Metals Confined in Time and Nanometer Space of Different Shapes"*, Acc. Chem. Res., 34 (2001), 257-264

[39] J. Chen, C. Glaus, R. Laforest, Q. Zhang, M. Gidding, M. J. Welch & Y. Xia: *"Gold Nanocages as Photothermal Transducers for Cancer Treatment"*, Small 6 (2010), 811-817

[40] S. Nie & S. R. Emory: *"Probing Single Molecules and Single Nanoparticles by Surface-Enhanced Raman Scattering"*, Science 275 (1997), 1102-1106

[41] A. Sinha, K. Suzuki, M. Takahara, H. Azuma, T. Nonaka & K. Fukumoto: *"Mesostructured Manganese Oxide/Gold Nanoparticle Composites for Extensive Air Purification"*, Angew. Chem. Int. Ed. 46 (2007), 2891-2894

[42] J.J. Storhoff, C.A. Mirkin: *"Programmed Materials Synthesis with DNA"*, Chem. Rev. 99 (1999), 1849-1862

[43] A. Kuzyk, R. Schreiber, Z. Fan, G. Pardatscher, E.-M. Roller, A. Högele, F. Simmel, A. Govorov & T. Liedl: *"DNA-based Self-Assembly of Chiral Plasmonic Nanostructures with Tailored Optical Response"*, Nature 483 (2012), 311-314

[44] A. P. Alivisatos, K. P. Johnsson, X. G. Peng, T. E. Wilson, C. J. Loweth, M. P. Bruchez, P. G. Schultz: *"Organization of 'nanocrystal molecules' using DNA"*, Nature 382 (1996), 609-611.

[45] W. Parak, T. Pellegrino, C. Micheel, D. Gerion, S. C. Williams & A. P. Alivisatos: *"Conformation of Oligonucleotides Attached to Gold Nanocrystals Probed by Gel Electrophoresis"*, Nano Lett. 3 (2003), 33-36

[46] S. Park: *"Characterization of Nanoparticle-DNA Conjugate and Control of DNA Conformation on Particle Surface*, PhD thesis, Massachusetts institute of technology (2009)

[47] D.D. Eley & D.I. Spivey.: *"Semiconductivity of organic substances -Part 9. Nucleic acid in the dry state"*, Trans. Faraday Soc. 58 (1962), 411

[48] D. Porath, G. Cuniberti, R. Di Felace: *"Charge transport in DNA-based devices"*. Top. Curr. Chem. 237 (2004), 183-227

[49] S. Tuukkanen, A. Kuzyk, J. J. Toppari, V. P. Hytönen, T. Ihalainen & P. Törmä, *"Dielectrophoresis of nanoscale double-stranded DNA and humidity effects on its electrical conductivity"*, Appl. Phys. Lett. 87 (2005)

[50] R.A. Marcus & Norman Sutin: *"Electron transfers in chemistry and biology"*, Biochimica et Biophysica Acta 811 (1985), 265-322

[51] Masateru Taniguchi & Tomoji Kawai (2006): *"DNA electronics"*, Physica E 33 (2006), 1-12

[52] C.J. Murphy, M.R. Arkin, Y. Jenkins, N.D. Ghatlia, S.H. Bossmann, N.J. Turro, J.K. Barton: *"Long-range photoinduced electron transfer through a DNA helix"*, Science, New series 262 (1993), 1025-1029

[53] J.K. Barton, C.V. Kumar & N.J. Turro (1986): *"DNA-Mediated Photoelectron transfer reactions"*, J. Am. Chem. SOC. 108 (1986), 6391-6393

[54] S.O. Kelley & J.K. Barton: *"Electron Transfer Between Bases in Double Helical DNA"*, Science 283 (1999), 375-381

[55] Tashica T. Williams, Duncan T. Odom & Jacqueline K. Barton: *"Variations in DNA Charge Transport with Nucleotide Composition and Sequence"*, J. Am. Chem. Soc. 122 (2000), 9048-9049

[56] Eric Meggers, Maria E. Michel-Beyerle & Bernd Giese: *"Sequence dependent long range hole transport in DNA"*, J. Am. Chem. Soc. 120 (1998), 12950-12955

[57] B. Giese, J. Amaudrut, A.-K. Kohler, M. Spormann & S. Wessely: *"Direct observation of hole transfer through DNA by hopping between adenine bases and by tunnelling"*, Nature 412 (2001), 318-320

[58] B. Giese: *"On the mechanism of long-range electron transfer through DNA"*, Angew. Chem. Int. Edn Engl. 38 (1999), 996-998

[59] M. A. O'Neill & J. K. Barton: *"DNA Charge Transport: Conformationally Gated Hopping through Stacked Domains"*, J. Am. Chem. Soc. 126 (2004), 11471-11483

[60] E. M. Boon, A. L. Livingston, N. H. Chmiel, S. S. David & J. K. Barton: *"DNA-mediated charge transport for DNA repair"*, PNAS 100 (2003), 12543-12547

[61] H. Ibach, H. Lüth: *"Solid-state physics: An introduction to principles of material science"*, 4th edition (2009), Springer, ISBN 978-3-540-93803-3

[62] S. S. Mallajosyula & S. K. Pati: *"Toward DNA Conductivity: A Theoretical Perspective"*. J. Phys. Chem. Lett. 1 (2010), 1881-1894

[63] H.-W. Fink & C. Schönenberger: *"Electrical conduction through DNA molecules"*, Nature 398 (1999), 407-410

[64] P. J. de Pablo et al: *"Absence of DC-Conductivity in λ-DNA"*, Physical review letters 85 (2000), 4992-4995

[65] A. Yu. Kasumov, D. V. Klinov, P.-E. Roche, S. Guéron & H. Bouchiat: *"Thickness and low-temperature conductivity of DNA molecules"*, Applied Physics Letters 84 (2004), 1007-1008

[66] D. Porath, A. Bezryadin, S. de Vries & C. Dekker: *"Direct measurement of electrical transport through DNA molecules"*, Nature 403 (2000), 635-638

[67] S. Bhattacharya, J. Choi, S. Lodha, D. B. Janes, A. F. Bonilla, K. J. Jeong & G. U. Lee: *"Electronic Conduction in DNA attached to Gold Electrodes"*, Nanotechnology 1 (2003), 79-82

[68] N. P. A. M. Briman, G. Andgruner: *"Charge transfer and charge transport on the double helix"*, Phys. Stat. Sol. 241 (2004), 69-75

[69] J. Gu, L. Cai, S. Tanaka, Y. Otsuka, H. Tabata, T. Andkawai: *"Electric conductivity of dye modified DNA films with and without light irradiation in various humidities"*, J. Appl. Phys. 92 (2002), 2816

[70] A. Terawaki, Y. Otsuka, H. Lee, T. Matsumoto, H. Tanaka & T. Kawai: *"Conductance measurement of a DNA network in nanoscale by point contact current imaging atomic force microscopy"*, Applied Physics Letters 86 (2005), 113901

[71] T. Kleine-Ostmann, C Jördens & K. Baaske: *"Conductivity of single-stranded and double-stranded deoxyribose nucleic acid under ambient conditions: The dominance of water"*, Appl. Phys. Lett. 88 (2006), 102102

[72] M. H Zareie, P. B. Andlukins: *"Atomic-resolution STM structure of DNA and localization of the retinoic acid binding site"*. Biochem. Biophys. Res. Commun. 303 (2003), 153

[73] B. Xu, P. Zhang, X. Li & N. Tao: *"Direct Conductance Measurement of Single DNA Molecules in Aqueous Solution"*, Nano Letters 4 (2004), 1105-1108

[74] A. B. Kotlyar, N. Borovok, T. Molotsky, H. Cohen, E. Shapir & D. Porath: *"Long, Monomolecular Guanine-Based Nanowires"*, Adv. Mater. 17 (2005), 1901-1905

[75] J. T. Davis & G. P. Spada: *"Supramolecular architectures generated by self-assembly of guanosine derivatives"*, Chem. Soc. Rev. 36 (2007), 296-313

[76] S.-P. Liu, S. Weisbrod, Z. Tang, A. Marx, E. Scheer & A. Erbe: *"Direct Measurement of Electrical Transport Through G-Quadruplex"*, Angew. Chem. Int., 49 (2010), 3313-3316

[77] J. Yguerabide & E. E. Yguerabide: *"Light-scattering submicroscopic particles as highly fluorescent analogs and their use as tracer labels in clinical and biological applications"*, Anal. Biochem. 262 (1998), 137-156

[78] L. M. Demers, C. A. Mirkin, R. C. Mucic, R. A. Reynolds, R. L Letsinger, R. Elghanian & A. G. Viswanadham: *"Fluorescence-based method for determining the surface coverage and hybridization efficiency of thiol-capped oligonucleotides bound to gold thin films and nanoparticles"*, Anal. Chem. 72 (2000), 5535-5541

[79] X. Liu, M. Atwater, J. Wang, Q. Huo: *Extinction coefficient of gold nanoparticles with different sizes and different capping ligands"*, Colloids and Surfaces B: Biointerfaces 58 (2007), 3-7

[80] J. Yguerabide & E. E. Yguerabide: *"Light-scattering submicroscopic particles as highly fluorescent analogs and their use as tracer labels in clinical and biological applications"*, Anal. Biochem. 262 (1998), 137-156

[81] I. Lubitz & A. Kotlyar: *"Self-Assembled G4-DNA-Silver Nanoparticle Structures"*, Bioconjugate Chem. 22 (2011), 482-487

[82] S. Halamish, G. Eidelshtein & A. Kotlyar: *"Plasmon-coupled nanostructures comprising finite number of gold particles"*, Plasmonics 8 (2013), 745-748

[83] I. Lubitz & A. Kotlyar: *"G4-DNA-cpated gold nanoparticles: synthesis and assembly"*, Bioconj. Chem. 22 (2011), 2043-2047

[84] Sampo Tuukkanen: *"Dielectrophoresis as a tool for on-chip positioning of DNA and electrical characterization of nanoscale DNA"*, Academic Dissertation for the Degree of Doctor of Philosophy, (2006)

[85] T. B. Jones: *"Electromechanics of particles"*, Cambridge University Press, Cambridge, (1995), ISBN 978-2869-01-5

[86] C. Zhang, K. Khoshmanesh, A. Mitchell & K. Kalantarzadeh: *"Dielectrophoresis for manipulation of micro/nano particles in microfluidic systems"*, Anal. Bioanal. Chem. 420 (2010), 396-401

[87] A. Csáki, S. Berg, C. Leiterer, R. Kretschmer, A. Wolff & W. Fritzsche: *"Integration of molecular structures in electrode gaps by dielectrophoresis"*. Proc. SPIE 7035 (2008), 5

[88] C. Holste, A. Sondermann, R. Moller & W. Fritzsche: *"Coupling G-Wires to metal nanoparticles"*, In DNA-BASED MOLECULAR ELECTRONICS:

International Symposium on DNA-Based Molecular Electronics. AIP 725 (2004), 53-57

[89] L. Zheng, J. P. Brody & P. J. Burke: *"Electronic manipulation of DNA, proteins, and nanoparticles for potential circuit assembly"*, Biosensors and Bioelectronics 20 (2004), 606-619

[90] N. G. Green, A. Ramos, A. Gonz´alez, H. Morgan & A. Castellanos: *"Fluid flow induced by nonuniform ac electric fields in electrolytes on microelectrodes: Observation of streamlines and numerical simulation"*. Phys. Rev. E 66 (2002)

[91] O. Z. Stern: *"Zeitschrift für Elektrochemie and angewandte physikalische Chemie"*, Elektrochem 30 (1924), 508-516

[92] A. Kuzyk, B. Yurke, J.J. Toppari, V. Linko & P. Törmä: *"Dielectrophoretic Trapping of DNA Origami"*, Small 4 (2008), 447

[93] S. Tuukkanen, A. Kuzyk, J.J. Toppari, H. Häkkinen, V.P. Hytönen, E. Niskanen, M. Rinkiö & P. Törmä: *"Trapping of 27 bp - 8 kbp DNA and immobilization of thiol-modified DNA using dielectrophoresis"*, Nanotechnology 18 (2007), 295204

[94] T. Parviainen, G. Eidelshtein, A. Kotlyar & J.J. Toppari: *"Conductive behaviour of G4-DNA-silver nanoparticle structures"*. Book chapter in *"Guanine Quartets: Structure and Application"*, ISBN: 978-1-84973-695-4, (2013)

[95] I. Diez-Perez, J. Hihath, T. Hines, Z.-S. Wang, G. Zhou, K. Müllen & N. Tao: *"Controlling single-molecule conductance through lateral coupling of π-orbitals"*, Nature nanotechnology 6 (2011), 226-231

[96] A. Kuzyk: *"Molecular devices for nanoelectronics and plasmonics"*, PhD Dissertation, University of Jyväskylä, (2009)

[97] N. Borovok, N. Iram, D. Zikich, J. Ghabboun, G. Livshits, D. Porath & A. Kotlyar: *"Assembling of G-strands into novel tetra-molecular parallel G4-DNA nanostructures using avidin-biotin recognition"*, Nucleic Acids Res. 36 (2008), 5050-5060

[98] N. Pastor: *"The B- to A-DNA Transition and the Reorganization of Solvent at the DNA Surface"*. Biophys J. 88 (2005), 3262-3275

[99] J. Vesenka, T. Marsh, E. Henderson & C. Vellandi: *"The diameter of duplex and quadruplex DNA measured by scanning probe microscopy"*, Scanning Microscopy 12 (1998), 329-342

[100] M. Di Ventra & M. Zwolak: *"DNA electronics"*, Encyclopedia of Nanoscience and Nanotechnology 2 (2004), 475-493

[101] V. Linko, S.-T. Paasonen, A. Kuzyk, P. Törmä & J. Toppari: *"Characterization of the Conductance Mechanisms of DNA Origami by AC Impedance Spectroscopy"*, Small 5 (2009), 2382-2386

[102] C. H. Hamann & W. Vielstich: *"Electrochemistry"*, Wiley-VCH, Weinheim, (1998)

[103] J. Bonnet, M. Colotte, D. Coudy, V. Couallier, J. Portier, B. Morin & S. Tuffet: *"Chain and conformation stability of solid-state DNA: implications for room temperature storage"*, Nucleic Acids Res. 38 (2010), 1531-1546

[104] S. Paasonen: *"Conductivity measurements of DNA TX tile and origami structures"*, Pro Gradu, University of Jyväskylä (2011)

[105] S. Tuukkanen, A. Kuzyk, J. J. Toppari, V. P. Hytönen, T. P. Ihalainen & P. Törmä: *"Dielectrophoresis of nanoscale double-stranded DNA and humidity effects on its electrical conductivity"*, Appl. Phys. Lett. 87 (2005), 183102

[106] H. Cohen, T. Sapir, N. Borovok, T. Molotsky, R. Di Felice, A. B. Kotlyar & D. Porath: *"Polarizability of G4-DNA Observed by Electrostatic Force Microscopy Measurements"*, Nano Letters 7 (2007), 981-986

[107] Ai-Min Guo, Zhi Yang, Hong-Jun Zhu and Shi-Jie Xiong: *"Influence of backbone on the charge transport properties of G4-DNA molecules: a model-based calculation"*, J. Phys.: Condens. Matter 22 (2010), 065102

[108] X. Guo, A. Gorodetsky, J. Hone, J. Barton & C. Nuckolls: *"Conductivity of a single DNA duplex bridging a carbon nanotube gap"*, Nature nanotechnology 3 (2008), 163

[109] T. Douki, J.-L. Ravanat, D. Angelov, J.R. Wagner & J. Cadet: *"Effects of duplex stability on charge-transfer efficiency within DNA"* Top. Curr. Chem 236 (2004), 1

[110] J. Cadet, T. Douki, D. Gasparutto & J.L. Ravanat: *"Oxidative damage to DNA: formation, measurement and biochemical features"*, Mutat. Res. 531 (2003), 5-23

[111] C. Yamahata, D. Collard, T. Takekawa, M. Kumemura, G. Hashiguchi & H. Fujita: *"Humidity Dependence of Charge Transport through DNA Revealed by Silicon-Based Nanotweezers Manipulation"*, Biophysical Journal 94 (2008), 63-70

Appendixes

Appendix A
Additional measured I-V characteristics

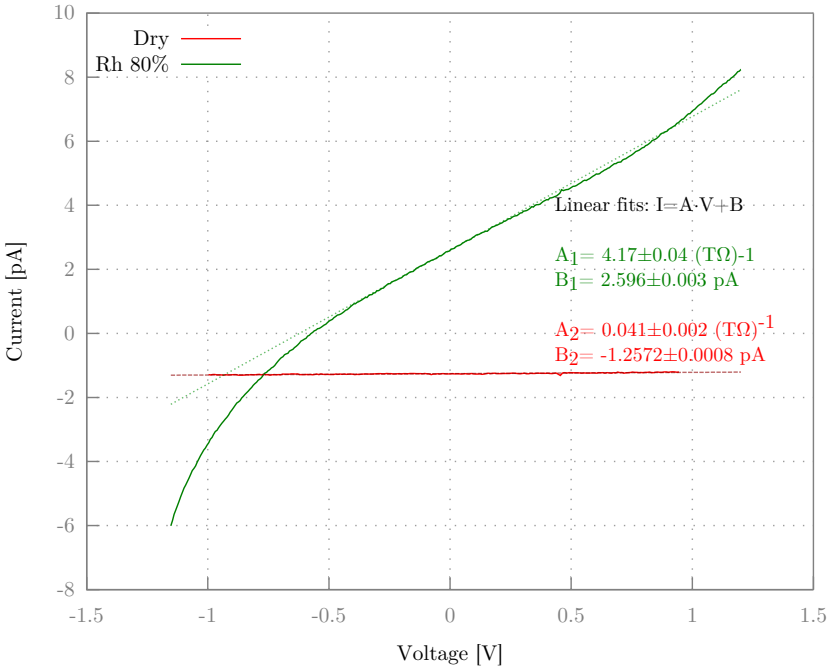

Figure 5.1. *I-V characteristics of an empty sample in increasing RH. The sample underwent the trapping procedure with no DNA-NP conjugates. The resistances at* 0.1 V *calculated by fitting a straight line into the data at the range of* 0.05-0.15 V

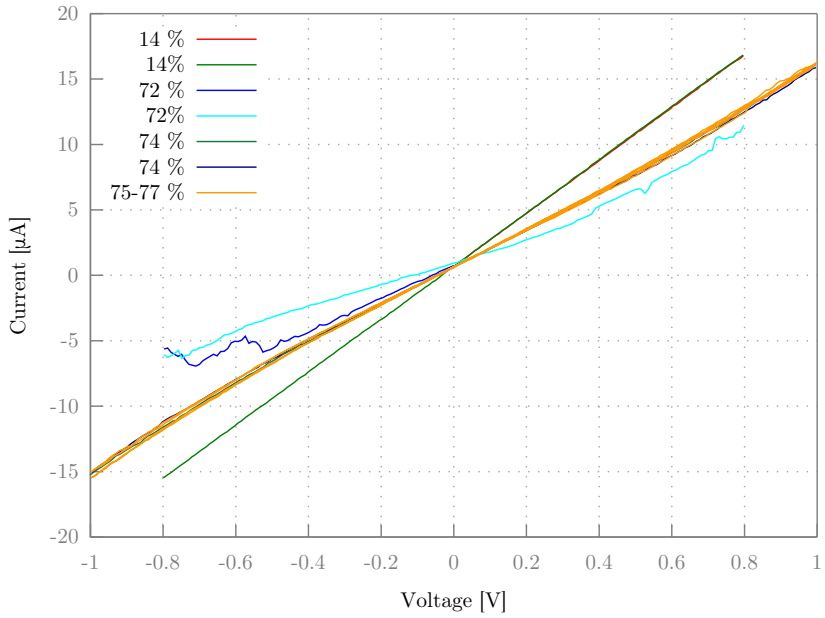

Figure 5.2. *I-V characteristics of a control sample with trapped citrate-capped AuNPs without conjugated G4-DNA. The resistances is of the order of* $50\,\mathrm{k}\Omega$ *regardless of the RH. The resistance corresponds to the resistance of the electrodes, meaning that the resistance of the AuNPs is of the order of* $1\,\mathrm{k}\Omega$ *corresponding to the high conductivity state of the AgNP chains.*